ELSEVIER

Journal of Power Sources 93 (2001) 234–257

JOURNAL OF POWER SOURCES

www.elsevier.com/locate/jpowsour

Influence of grid alloy and fast charge on battery cycle life and structure of the positive active mass of lead acid batteries

M. Dimitrov, D. Pavlov*

Central Laboratory of Electrochemical Power Sources, Bulgarian Academy of Sciences, Sofia 1113, Bulgaria

Received 27 March 2000; received in revised form 12 August 2000; accepted 4 September 2000

Abstract

It has been found experimentally that during cycling the pore volume in PAM increases. The fraction of macropores ($r > 10$ μm) may reach up to 30–40% of the pore volume, whereas that of micropores ($r < 0.1$ μm) decreases. The BET surface area is reduced. The size of the crystallites in the crystal zones of lead dioxide particles increases. If the grid alloy contains Sb its concentration in PAM increases on cycling, which leads to a decrease in particle and crystallite size. The degree of these changes in PAM structure is determined by the charging current density as well as by the amount of Sb and Sn in the grid alloy and in PAM. When the charge is conducted with high currents ($I \geq 1.5$ C) the role of Sb and Sn in PAM decreases substantially. On fast charge and at Sb content higher than 0.2 wt.%, PbO_2 crystallites sized between 40 and 60 nm are formed. On slow charge of plates with pure Pb grids, these values are 90–100 nm. The capacity is influenced by the structure of the aggregates and particles in PAM as well as by their degree of crystallinity. On fast charge, more crystallites are formed in the particles, which improves the contact between the latter's crystal zones thus interconnecting them into an integral network of crystal zones with uniform electron conductivity throughout the volume of PAM. Consequently, the capacity of the plates is maintained high for a longer period of time. The evolution of this structure on cycling has been followed as well as its effect on the capacity of the positive plates. The phenomena that limit the life of the positive plates are: (a) breaking of the skeleton, (b) formation of crystal particles with poor contact between them, (c) formation of a membrane layer on the surface of the aggregates, and (d) deterioration of the agglomerate structure. It was also found that neither the charge mode nor the presence of additives affect the loss of PAM density on cycling. In order to improve the cycle life of the positive plates they should be charged with high current ($I_1 \geq 1.5$ C). This requirement is not obligatory if the grid alloy contains sufficient amounts of Sb and Sn. The influence of charging current on PAM structure and hence on plate life is interpreted on grounds of a sol–gel–crystal mechanism of the processes that take place on battery charge.

Keywords: Lead acid battery (LAB); Lead dioxide; LAB positive plate; LAB cycle life; LAB charging mode; LAB alloys

1. Introduction

The phenomena that determine the capacity and cycle life of the positive plates of lead acid batteries (LAB) proceed in the lead dioxide active mass (PAM) and in the interphase layer between current collector (metal grid) and PAM. It has been demonstrated recently that the high charge rate (0.5–1.0 C and above) of LAB improves the capacity and the life of the positive plates on deep discharge cycling [1–9]. Combined with confinement of the active material volume (long known tubular design or appropriate level of compression) [10] (references in [11]), this seems to resolve largely the cycle life problem of the positive plates of LAB. At low rate of charge, however, the presence of antimony and tin as grid alloying additives or in the active material, and/or the addition of H_3PO_4 to the electrolyte have proved essential for the satisfactory plate performance [12–18]. It has also been established that H_3PO_4 and Sb act as crystal growth modifiers [19–21].

The evolution of PAM structure throughout battery cycle life has been extensively studied. Phenomena such as formation of larger PAM particles [21–25] or decline of their electrochemical activity due to decreased hydrogen content in the PbO_2 lattice [26–30], transformation of the PAM pore system into a non-homogeneous one with coarse voids and coralloid PbO_2 structure [31–34] have been pointed out as determining the cycle life of the positive plates.

A good correlation between PAM conductivity and its utilization has been found [8–10,33,35]. The aggregate-of-spheres (AOS) model has been elaborated [2], which regards PAM as a periodic array of contacting spheres. The conductivity of AOS is supposed to depend on the ratio of the neck to sphere radii. Recent developments of the model

* Corresponding author. Tel.: +359-2-718651; fax: +359-2-731552.
E-mail address: dpavlov@mbox.cit.bg (D. Pavlov).

0378-7753/01/$ – see front matter
PII: S0378-7753(00)00598-X

consider also the nucleation and growth of PbO_2 particles [36,37].

In some earlier papers of ours [38–41] we tried to distinguish the effect of the structure and properties of the grid/PAM interphase layer from those of PAM itself. When $PbSO_4$ crystals or caverns are formed in the interphase layer and/or only a limited number of bridges (branches of the PAM skeleton) connect PAM with the corrosion layer, the capacity is limited by the interphase layer [39]. Such a structure was named ''inefficient interphase layer structure'' or ''interphase layer effect'' replacing the more general term ''PCL effect'' [38]. When the PAM is the capacity limiting element, the plate structure was termed ''normal''. It was established that the cycle life of the lead dioxide electrode was proportional to the current density during the initial effective stage of charge in case of normal plate structure [38].

The aim of the present paper is to investigate the behavior of positive plates with normal structure. An attempt will be made to answer the following questions:

1. How do fast and slow charge influence the structure of PAM and the system of pores in PAM, as well as the cycle life of the battery?
2. What is the influence of the grid alloying additives (particularly Sb and Sn) on the structure of PAM and the cycle life of the positive plates?

In short, the aim of the present paper is to disclose the nature of the phenomena that determine the dependence of battery performance parameters on charge algorithm and alloying additives.

2. Experimental

2.1. Battery manufacture and testing

Motorcycle batteries (12 V) with two positive and three negative plates per cell were manufactured using 3BS paste. The positive grids were cast from Pb, Pb–4% Sb, Pb–1.8% Sb–0.3% Sn or Pb–0.06% Ca–1.3% Sn alloys. The negative grids were pure Pb ones. After formation, the PAM density was 4.0 g/cm^3. Absorptive glass mat (AGM) separator was used, which slows down the swelling of the active masses on cycling. The AGM was under 25% compression (i.e. under a pressure of 20 kPa). This compression is lower than the optimum value [10] so as to allow the PAM to expand. The cells were of the flooded type with H_2SO_4 solution of s.g. 1.28. Further in the text the battery type will be denoted by the alloy of the positive grids. The batteries were charged at slow and fast charge modes.

2.1.1. Slow charge cycling

One battery (12 V/8.15 A h) with pure Pb grids and another one (12 V/8.8 A h) with PbSb grids were set to cycling at charging current $I = 0.55$ A. The charge factor was constant $F_{ch} = 1.2$ (charge time 18 and 19 h, respectively).

A 12 V/9 A h battery with PbSbSn grids and another one (12 V/9.5 A h) with PbCaSn grids were charged according to the CC/CV/CC scheme with $I_1 = 2$ A, $U_2 = 15.0$ V, $I_3 = 0.4$ A, and $F_{ch} = 1.15$.

The discharge current was

- 1.65 A ($I = 22.7$ mA/g PAM) for the batteries with pure Pb grids;
- 1.75 A ($I = 22.5$ mA/g PAM) for the batteries with PbSb grids;
- 2.0 A ($I = 23.8$ mA/g) for the batteries with PbSbSn and PbCaSn grids.

The batteries were discharged down to 11 V, i.e. 1.83 V per cell.

2.1.2. Fast charge cycling

The charge period was divided in three stages following the scheme CC/CV/CC. The charging current during the initial effective stage was $I_1 = 12$ A (approximately $1.5C_0$). Charging was conducted until the battery voltage reached 15.3 V for Pb and Pb–4% Sb batteries, and then continued at a constant voltage of $U_2 = 15.3$ V. The current decreased and when it reached 0.2 A the final CC period began with $I_3 = 0.2$ A ($0.02C_0$). The charging regime for both the PbCaSn and PnSbSn batteries was $I_1 = 12$ A (approximately $1.3C_0$), $U_2 = 15$ V, and $I_3 = 0.4$ A.

Discharge of the battery with pure Pb grids was conducted with a current $I = 1.65$ A ($\sim 0.2C_0$; $I = 22.7$ mA/g PAM) down to a cut-off voltage $U_{fin} = 11$ V (1.83 V per cell). The battery with PbSb grids was discharged with a current $I = 1.75$ A ($I = 22.5$ mA/g PAM) down to the same cut-off voltage. The batteries with PbCaSn and PbSbSn grids were discharged with $I = 2$ A ($\sim 0.2C_0$; $I = 23.8$ mA/g). The time of discharge was about 5 h for all types of batteries.

2.2. Investigations of the changes in PbO_2 structure and in PAM pore system during cycling

Samples were taken periodically during the cycling test and set to XRD examinations, mercury porosimetry, BET surface area determination and atomic absorption spectrometry to determine the structure and phase composition of the PAM as well as the Sb content in it. X-ray diffractograms were recorded at $0.02 \times 2\theta$ steps with 2 s per step. The peaks were fitted with Voigt function and the crystallite size was estimated from full width at half maximum (FWHM) of the (0 0 2) β-PbO_2 peak according to the Sherrer equation.

3. Experimental results

3.1. Cycle life test results

The results from the cycle life tests of the batteries with Pb and Pb–4% Sb grids at slow and fast charge regimes are

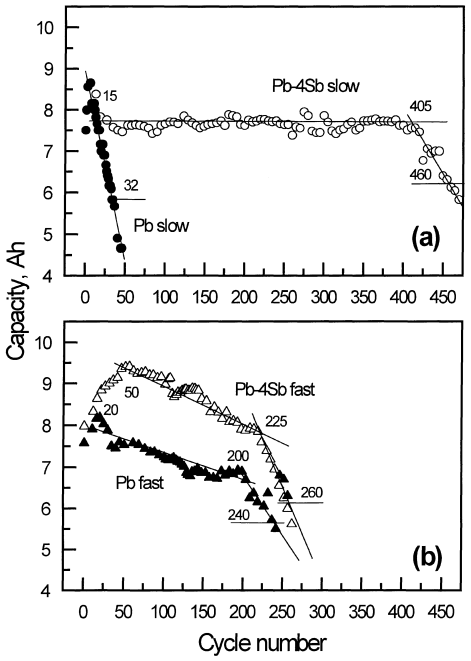

Fig. 1. Cycle life of positive plates with Pb and Pb–4% Sb grids: (a) slow charge; (b) fast charge.

presented in Fig. 1, and those for the batteries with PbSnSb and PbSnCa grids are given in Fig. 2. The end of battery life criterion was assumed to be when the battery failed to deliver 70% of its rated capacity. The number of cycles at the end of battery life is given close to the respective curves.

The following conclusions can be drawn from the figures.

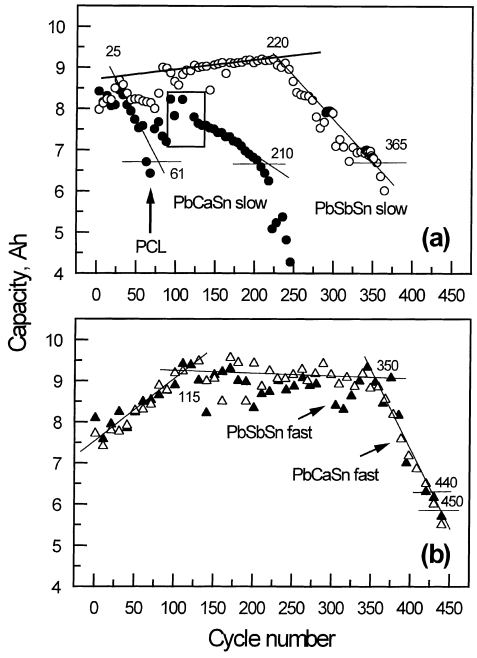

Fig. 2. Cycle life of positive plates with PbCaSn and PbSbSn grids: (a) slow charge; (b) fast charge. Marked area is enlarged in Fig. 3.

3.1.1. Cycle life periods

During formation of the plates, the cured paste comprising basic lead sulfate and PbO is converted into lead dioxide active mass. Let us name the structure of this positive active mass "technological" as it is related to the technology of plate manufacture. On battery cycling, the technological structure of PAM disintegrates partially on discharge ($PbO_2 \rightarrow PbSO_4$) and a new structure is built on charge ($PbSO_4 \rightarrow PbO_2$), which can be called "operative". The technological structure needs a certain number of cycles to transform fully into operative one. On further cycling, the operative structure of PAM undergoes evolution. Depending on the conditions of charge and discharge, unfavorable changes may occur in the PAM structure, which may limit the cycle life of the battery.

Judging by the capacity curves the cycle life of the batteries can be divided into three periods:

1. *Initial period* ("*youth*"): during this period formation of the active material is completed and the structures of PAM and of the interphase layer, built during plate formation, are transformed into operative structures formed on charge/discharge cycling. Typically, the capacity rises during this period. It is evident from Fig. 1 that the plates with Pb grids cycled at low charge rate lose rapidly their capacity and "die in their youth" as a result of inefficient structure of the interphase layer.
2. *Middle period*: during this period the structures of PAM and of the interphase layer are partially destroyed and rebuilt, more or less reversibly, during discharge and charge. The capacity of the plates remains constant as seen in Fig. 1a (Pb–4% Sb (slow)) and Fig. 2b (PbSbSn (fast); PbCaSn (fast)). When certain irreversible changes in the structures take place the capacity decreases slowly (Fig. 1: Pb–4% Sb (fast); Pb (fast)).
3. *Final period* ("*old age*"): during this period irreversible processes take place, which lead to the end of plate life. These processes are related to
   - substantial thinning or breaking of the current collectors due to corrosion;
   - changes in the macrostructure of PAM as a result of which parts of it are excluded from the current generation process; the connections between the different zones in PAM break down progressively and the current-carrying system in the plate disintegrates;
   - loss of conductivity of the interphase layer between PAM and the current collector as a result of formation of $PbSO_4$ crystals (which are not oxidized) and/or formation of cracks and caverns in this layer;
   - electrochemical reactivity of PbO_2 particles.

Figs. 1 and 2 show the cycle numbers marking the above three periods, and Table 1 gives these numbers for the different batteries under test. It can be seen that there is no middle period in the cycle life of some batteries (Fig. 1: Pb (slow); Fig. 2: PbCaSn (slow)).

Table 1
Periods of positive plate life

Alloy	Charge mode	Cycle number				Group
		Cycle life	Initial period	Middle period	End period	
Pb	Slow	32	15		15–32	b
	Fast	240	20	20–200	200–240	c
Pb–4% Sb	Slow	460	15	15–405	405–460	a
	Fast	260	50	50–225	225–260	c
PbSnSb	Slow	365	25	25–220	220–365	c
	Fast	450	115	115–350	350–450	a
PbCaSn	Slow	210	25		25–210	b, c
	Fast	440	115	115–350	350–440	a

3.1.2. Phenomena that limit battery life

1. Batteries that have endured 440–470 cycles fail mainly because of corrosion of the collectors. They are cycled at
   Slow charge — Pb–4% Sb battery
   Fast charge — PbSnSb and PbCaSn batteries

2. Batteries with short cycle life are cycled at
   Slow charge — Pb plates (32 cycles)
   Slow charge — PbSnCa plates (65 cycles)

The life of these batteries is limited by the phenomena that take place in the interphase layer. During the initial period, an inefficient interphase layer structure has been built.

In order to verify the above assumption, the following experiment was performed with the battery with PbCaSn grids (Fig. 2a).

The cell that had the smallest capacity was replaced for a new one after the 72nd cycle. After that, the capacity of the battery increased from 6.5 to 8.5 A h, but soon after the replacement the capacity began to decline again. Then a special sequence of charges was applied and the results are presented in Fig. 3. It is an enlargement of the encircled segment of the capacity curve in Fig. 2a.

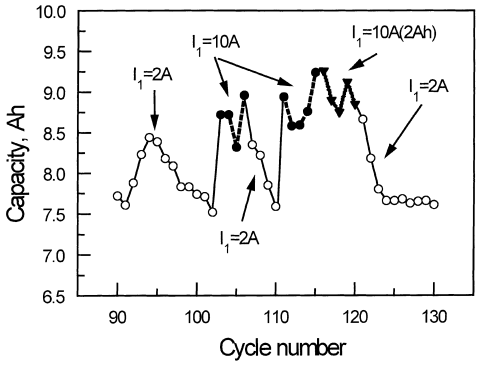

Fig. 3. Influence of the initial charge current on the capacity of the PbCaSn plate. Excerpt from Fig. 2.

After the capacity decreased to 7.5 A h (102nd cycle) we changed the charging current from 2 to 10 A (1.5 C) during cycles 103–106 (marked with black dots). The capacity increased from 7.5 to 8.75 A h. The influence of the charging current (I_1) during the effective charge stage is manifested in these four cycles. Then between cycles 107 and 110 the current I_1 was reduced back to 2.0 A (marked with white circles in Fig. 3). The capacity during these four cycles decreased from 8.4 to 7.6 A h. Obviously, the plates had preserved their liability to interphase layer passivation at low charging current. Then the charging current I_1 was once again increased to 10 A (marked with black dots in Fig. 3), the capacity rose again from 8.6 to 9.4 A h.

It was interesting to find whether the current of 10 A exerted an influence on the capacity throughout the entire effective charge stage until a voltage of 2.5 V per cell was reached or only at the beginning of this stage when mainly the interphase layer was charged. After 116 cycles (marked with triangles in Fig. 3) the battery was charged at 10 A until 2 A h were introduced into the cell. During these five cycles, the capacity preserved its high value between 8.75 and 9.1 A h. This fact indicates that the high charging current is most efficient at the beginning of charge, when the processes of charge occur at the interphase layer [38]. Hence, the decline in capacity of Pb and PbSnCa batteries is an interphase layer effect. Further charge of the battery was conducted with $I_1 = 2$ A. The battery endured 210 cycles before reaching its end of life.

3. Batteries with a cycle life longer than 65 cycles and shorter than 350 cycles:
   Slow charge — PbSnSb plate (365 cycles; Fig. 2a)
   Fast charge — Pb plate (240 cycles; Fig. 1b)
   Fast charge — Pb–4% Sb plate (260 cycles; Fig. 1b)

It could be expected that the life of these batteries would be limited by irreversible structural changes in PAM.

Fig. 1b shows that the fast charge prolongs the life of the plates with Pb grids making the interphase layer structure

more stable and conductive, but shortens the life of Pb–4% Sb plates from 460 to 260 cycles. During the middle cycle life period, the latter battery had a capacity higher by 1.5–2 A h as compared to its pure Pb counterpart, but in both plate types some structural processes have shortened the cycle life.

The data in Figs. 1–3 give grounds for the following general conclusion. There is an *optimum operative structure* of PAM and of the interphase layer, which ensures a constant capacity performance of the battery during the middle period of its cycle life. In this particular case the life of the battery is limited by corrosion of the current collector. This optimum operative structure is built and maintained by the technology of plate preparation, the charge mode and the presence of dopants in PAM and in the interphase layer.

3.2. Porosity measurements

3.2.1. Pore volume of PAM

Periodically during the cycling test a cell was removed from the battery and PAM samples were taken for XRD phase composition determination and crystallite size analysis, SEM observations, BET surface area determination and porometric measurements.

The changes in porosity on cycling are presented in Fig. 4. The pore volume of PAM for all batteries under test increases on cycling, which indicates that the active mass "opens" and becomes more accessible for the electrolyte. Fig. 4a shows that the pore volume curves obtained from the fast charge test of plates with Pb and Pb–4% Sb grids are steeper and at the end of life PAM has a pore volume of 0.28–0.29 cm^3/g. Fig. 4b shows that the same pore volume value (0.29 cm^3/g) is reached by the PAM of plates with PbSnSb grids when they are cycled at low charge rate. The data in Table 1 indicate that these three types of batteries belong to the group for which the changes in PAM structure are responsible for the end of life of the positive plates. On the other hand, Fig. 4b shows that the plates with PbCaSn and PbSnSb grids subjected to fast charge maintain a pore volume between 0.24 and 0.26 cm^3/g throughout the 200 cycles. This value does not limit the life of the battery plates. Hence, there is a critical value of about 0.27 cm^3/g above which the pore volume of PAM becomes a life limiting parameter for the positive plates. As evident from Fig. 4b the rate of expansion of the pore volume is equal for both fast and slow charge modes. On the other hand, the discharge mode is the same for the two batteries. Hence, it can be assumed that the observed pore volume increase is related to the discharge process.

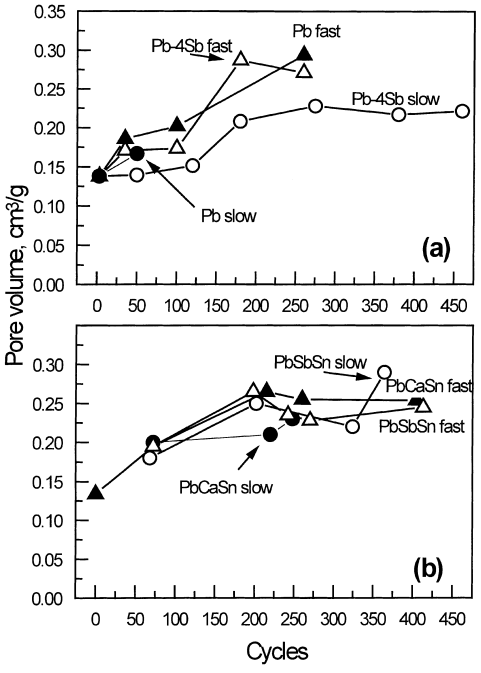

Fig. 4. Changes in pore volume of PAM during cycling: (a) plates with Pb or Pb–4% Sb grids; (b) plates with PbSbSn or PbCaSn grids.

3.2.2. Evolution of cumulative pore size distribution on cycling

The changes in cumulative pore size distribution on cycling of the batteries under test are presented in Fig. 5. The ordinate values are normalized against the highest pore volume value for each PAM sample. The porograms imply the following three characteristic features:

1. The micropores (with radii < 0.1 μm) in PAM subjected to slow charge constitute between 15 and 5% of the pore volume and change relatively slowly on cycling. During fast charge cycling the volume of the micropores decreases as follows: from 52 to 20% for the Pb battery, from 40 to 10% for the Pb–4% Sb one, from 28 to 18% for the PbSnSb one, and from 25 to 16% for the PbCaSn battery. The lack of correlation between these changes and battery life indicates that the quantity of micropores in PAM is not a life limiting parameter.
2. The number of pores with radii > 1 μm (macropores) increases on cycling. Their volume amounts to 30% of the pore volume for Pb–4% Sb plates at slow charge. The respective values for the other battery types are 33% for Pb (fast), 30% for Pb–4% Sb (fast), 63% for PbSnSb (slow), 29% for PbSnCa (slow), 42% for PbSnCa (fast), and 44% for PbSnSb (fast). If these values are correlated to the cycle life data presented in Table 1, we can conclude that the volume of macropores with radii > 1 μm, when less than 45% of the pore volume, is not a life limiting parameter. On cycling the PbSbSn (slow charge) battery the content of macropores increases from 40 to 63% between cycles 324 and 364 (Fig. 5c) and then they may limit the life of the battery. This is actually due to the increased resistance of PAM.
3. It is interesting to note that, between cycles 270 and 350 (Fig. 2a), the PAM of the PbSbSn battery (fast charge) preserves a constant capacity and contains 44% of

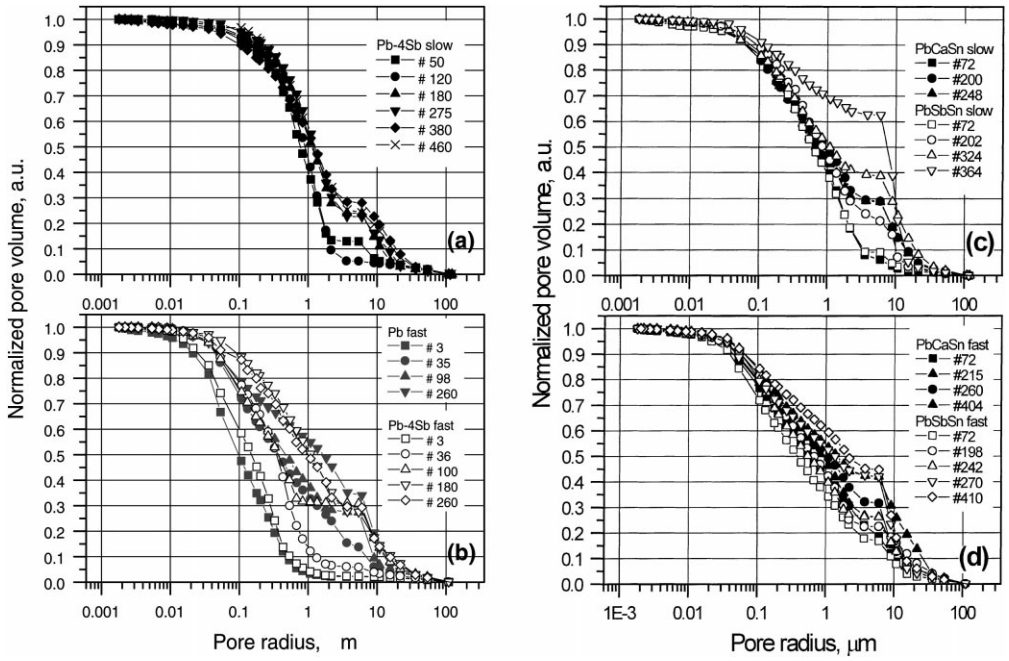

Fig. 5. Changes in cumulative pore size distribution on cycling of the batteries under test.

macropores ($r > 5$ μm) (Fig. 5d). Hence, it can be assumed that the main impact of the fast charge mode is that it keeps the connections between the branches of the PAM skeleton stable and intact even when 44% of the pores are macropores.

3.3. Changes in BET surface area on cycling

The changes in BET surface area of PAM during cycling of the batteries under tests are presented in Fig. 6.

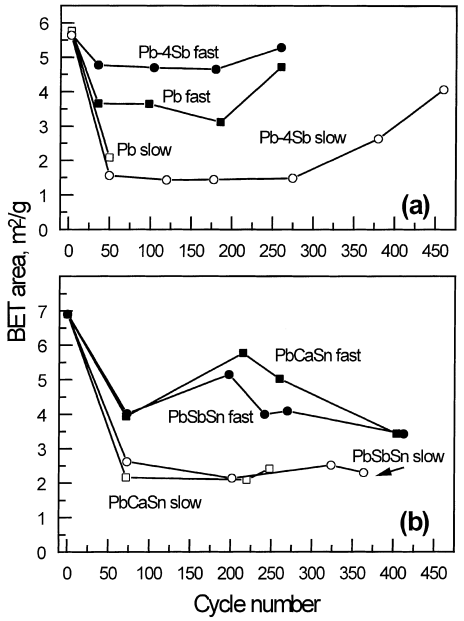

Fig. 6. Specific surface area (BET) of PAM during the cycling test.

The following conclusions can be drawn:

1. The surface area decreases during cycling from 6–7 m^2/g initially (as obtained during formation of PAM) to 3.5–5 m^2/g at fast charge and 1.5–2.5 m^2/g at slow charge for 50–60 cycles. When the operative structure of PAM is built up the BET surface area remains constant thereafter except in some cases. It is logical to assume that smaller PbO_2 particles are formed (large surface area of PAM) at fast charge than those obtained at slow charge (low surface area). It has been established earlier that the surface area of PAM is determined mainly by the surface of the micropores ($r < 0.1$ μm) [42]. Fig. 5 shows that at slow charge the quantity of micropores changes from 15 to 5%, while at fast charge it decreases from 52 to 10%. The larger quantity of micropores is responsible for the larger surface area of PAM (Fig. 6) on fast charge cycling versus that of PAM cycled at low charge rate.
2. If the BET surface area results for different plate types are correlated to the cycle life data presented in Table 1, it can be seen that the changes in BET surface area are not a life limiting parameter.

3.4. Structural investigations of PAM through X-ray diffraction

It has been established that PAM comprises β-PbO_2 crystals. It has also been found earlier that the lead dioxide particles consist of crystalline (PbO_2) zones and hydrated $PbO(OH)_2$ zones [43]. The crystalline zones contain a certain number of crystallites. The influence of charge mode on the size of β-PbO_2 crystallites was determined by the

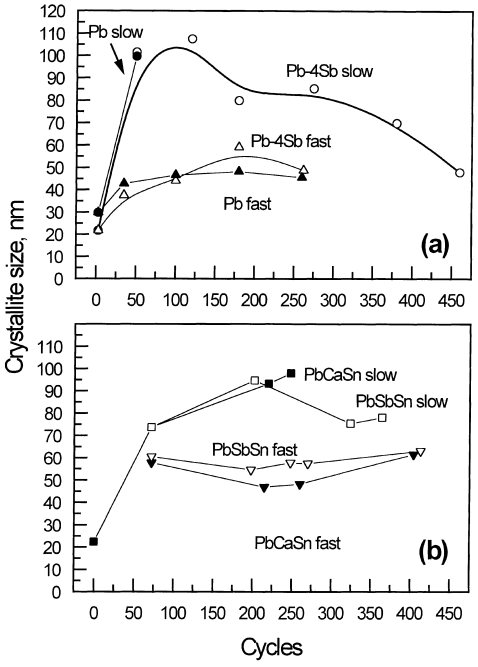

Fig. 7. Crystallite size (XRD) of PbO_2 during the cycle life test.

width at half XRD peak height for the PAM of all batteries under test. Fig. 7 shows the size of the β-PbO_2 crystallites after different cycling times for batteries subjected to fast and slow charge cycling.

The data in this figure give grounds for the following conclusions:

1. The PbO_2 crystallite size increases during the first 100 cycles for all types of positive plates. The PbO_2 crystallites are sized between 22 and 30 nm after formation. When slow charge cycling is employed the size of the crystallites increases to 70–107 nm, and for fast charged plates to 47–64 nm, respectively. The grid alloying additives influence the maximum size of the crystallites that can be reached during cycling.
2. The curves crystallite size/number of cycles for plates with Pb–4% Sb grids feature a maximum of 107 nm after 125 cycles at slow charge rate and 64 nm after 175 cycles at fast charge rate. The crystallite size decreases after the maximum on further cycling.
3. If the cycle life values for the batteries presented in Table 1 are compared with the data in Fig. 7, it can be seen that the life of the positive plates is not directly determined by the crystallites size.

3.5. Antimony content in PAM during cycling

The concentration of antimony in PAM on cycling was determined for all types of batteries with Sb grids. Fig. 8 presents the obtained results.

The accumulation of Sb in PAM particles depends on the antimony content in the grid alloy, the charge mode (fast or slow) and the number of cycles. The greatest amount of Sb (0.9 wt.%) was absorbed by the PAM of the plates with Pb–4% Sb grids at slow charge after 460 cycles.

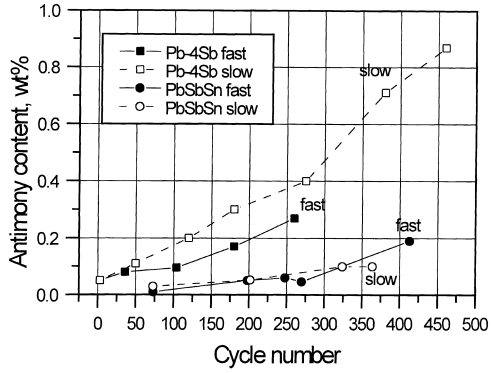

Fig. 8. Accumulation of antimony in PAM during the cycle life test.

If we combine the data in Figs. 7 and 8 we will obtain the correlation between the size of PbO_2 crystallites and the Sb content in PAM. These dependencies are presented in Fig. 9.

At 0.2% Sb content in the $PbO_2/PbO(OH)_2$ particles the size of PbO_2 crystallites depends on the charge mode. On fast charge cycling, PbO_2 crystallites of up to 60 nm are formed, whereas on slow charge the crystallites are larger than 100 nm. Obviously, at low Sb contents in the particles, the crystallites size depends on the mode of charge. On slow charge of Pb–4% Sb plates when the Sb content in the particles reaches 0.9%, the crystallites become equal in size to those in PAM cycled at high charge rate and containing less than 0.2% Sb.

3.6. SEM observations of the evolution of PAM during cycling

3.6.1. PAM structure

As determined earlier [22,43–45], the structure of PAM consists of two levels:

1. *Microstructural level*: the main building element is the PbO_2 particle comprising crystal (PbO_2) and hydrated

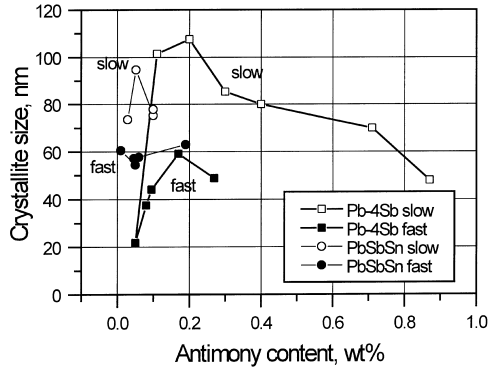

Fig. 9. PbO_2 crystallite size (XRD) dependence on antimony content in PAM.

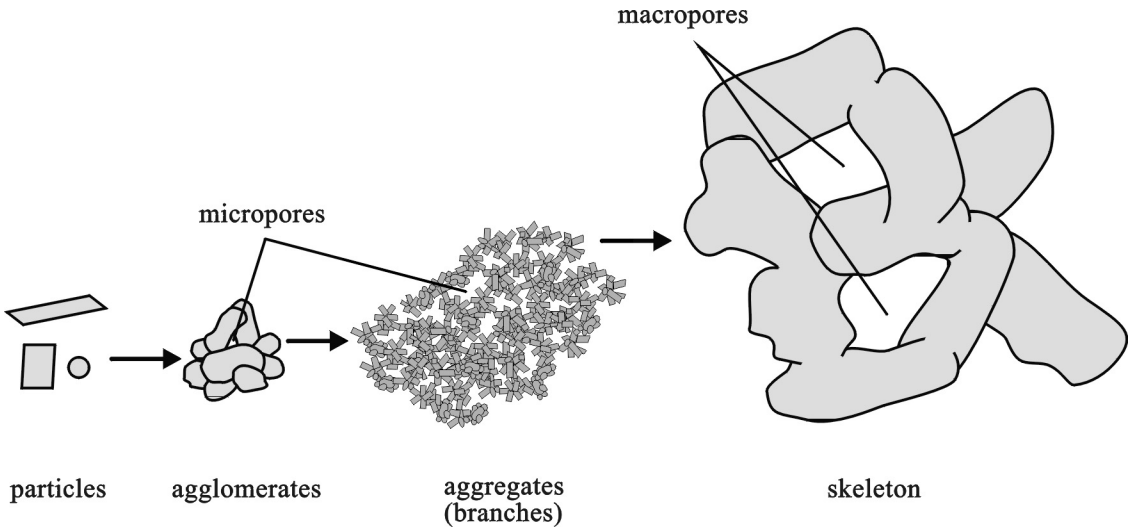

Fig. 10. Scheme of the basic structural elements of PAM.

($PbO(OH)_2$) zones; many particles interconnect to form agglomerates, which sometimes contain micropores.

2. *Macrostructural level*: the agglomerates are interconnected to form
   - a porous mass that contains micro- and macropores, or
   - aggregates (branches); macropores are formed between the aggregates and the latter are interconnected thus forming the skeleton of PAM.

The above structural elements are schematically presented in Fig. 10.

Which type of macrostructure will dominate depends on the phase composition and the structure of the cured paste, as well as on the cycling conditions during plate operation.

3.6.2. Initial structure of PAM obtained after formation of 3BS pastes

SEM micrographs of PAM formed from a 3BS precursor are presented in Fig. 11. The PAM consists of interconnected rounded agglomerates sized between 0.1 and 1 μm, and pores 0.2–0.6 μm in size between the agglomerates (Fig. 11a). The agglomerates are interconnected thus forming a porous mass.

At higher magnifications (20,000×, Fig. 11b) it can be seen that every agglomerate consists of particles of various size. Its morphology is better seen at 100,000× magnification in Fig. 11c. Numerous small spherical particles (∼30 nm) can be identified, together with some particles sized 100–200 nm at a more advanced stage of crystallization. Some of them have pronounced walls and edges.

3.6.3. Evolution of PAM structure on fast charge cycling of plates with PbSb grids

3.6.3.1. Macrostructure. Fig. 12 presents SEM photographs of the PAM macrostructure after 35, 100, 180 and 260 cycles at 300× magnification. The evolution of the structure on cycling will be considered below in correlation to the experimental results obtained by mercury porometry for the porosity (Fig. 4), the pore size distribution (Fig. 5) and the BET surface area (Fig. 6).

These considerations, together with the cycle life results (Fig. 1b), imply the following evolution of the structure of PAM on cycling:

1. 35th cycle (Fig. 12a): the PAM consists of agglomerates interconnected into a rather homogeneous porous mass. After 35 cycles, the pore volume increases from 0.14 to 0.17 cm^3/g and 4% of it is occupied by the newly formed pores with radii > 10 μm. The pores with $1 < r < 10$ μm constitute 8% of the pore volume. The capacity reaches its maximum value of 9.5 A h.
2. 100th cycle (Fig. 12b): aggregates begin to outline clearly during cycling and macropores are formed between them. They occupy 12% ($r > 10$ μm) of the volume and those with $1 < r < 10$ μm occupy 20%. Fig. 12b shows that the aggregate surface and the structure of its interior are built of agglomerates of the same kind and size. During this transformation, the capacity decreases from 9.5 to 9 A h.
3. 180th cycle (Fig. 12c): the pores have formed a well-developed ion transport system within PAM. The volume of the pores with $r > 10$ μm amounts to 18% of the pore volume and that of the pores with $1 < r < 10$ μm, to 32%. The pore volume is 0.28 cm^3/g, half of the volume being occupied by pores with $r > 1$ μm. The curves in Fig. 5 show that the volume of the micropores with $r < 0.1$ μm decreases from 25% at the 100th cycle to 11% at the 180th cycle, i.e. densification of aggregates has occurred. The surface of some aggregates is smoother and the agglomerates begin to detach from each other forming well outlined pores. As a result of these changes in PAM structure and in the pore system the capacity declines from 9 to 8 A h.

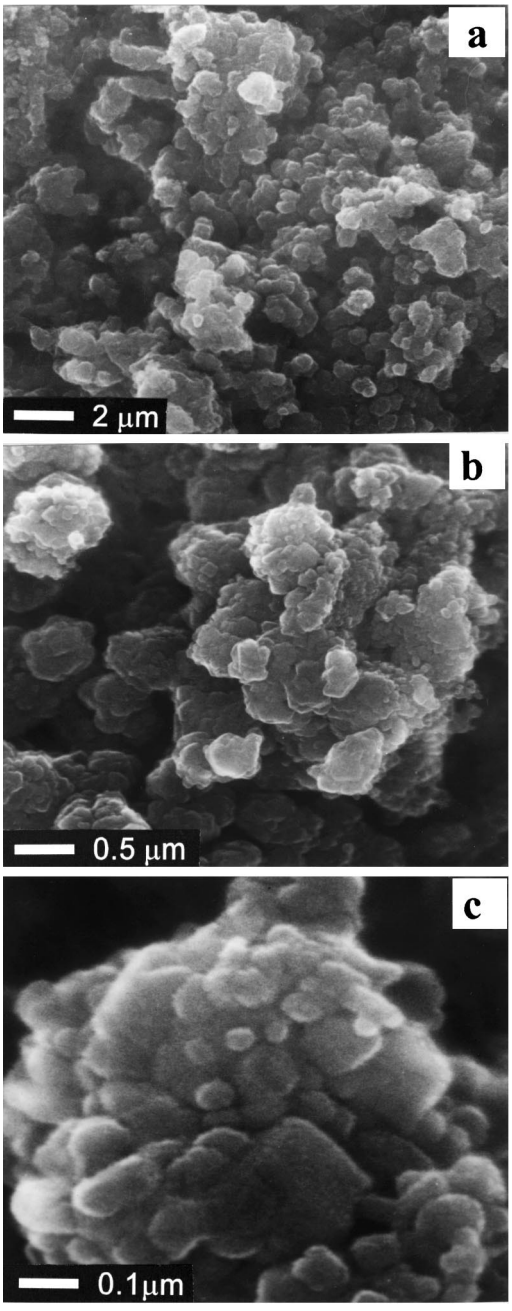

Fig. 11. SEM micrograph of as-formed (technological structure) of PAM obtained from 3BS precursor.

4. 260th cycle (end of cycle life): Fig. 1b indicates that after 225 cycles the final cycle life period starts and the capacity begins to decrease rapidly reaching the end of life at cycle 260. The photograph in Fig. 12d shows that the agglomerates on the aggregates' surface have stuck to each other in such a way that the aggregate's surface has become smooth. At some places the aggregates are cracked and the electric path through the skeleton is interrupted. The aggregates' density has increased. The rough parts of the aggregates are the sites where the sample was broken off. The interior of the aggregates is visible at these sites. It is highly microporous. The BET surface area is 5 m^2/g, i.e. it is high enough. The size of the crystallites ranges between 40 and 50 nm (Fig. 7). Figs. 4 and 5 show that the porous system does not change substantially between 180 and 260 cycles.

The above results show that at the end of plate life the PAM has large surface, nano-sized crystallites, very well developed porous system, but still the capacity is low and decreases on cycling. What could be the reason for this capacity loss?

1. The well developed macrotransport pores allow free access of H_2SO_4 to the interphase layer and on discharge the electric resistance of this layer increases before the PAM is fully discharged. This influence of the pore system of the operative PAM structure was established earlier [34].
2. The dense aggregates form a hard skeleton, which cannot accommodate the pulsation of PAM on charge and discharge and cracks are formed between the aggregates as a result of which large zones of PAM are excluded from the discharge process.
3. The highly compact surface layer of the aggregates impedes the access of H_2SO_4 and H_2O to their interior and hence a great part of the PbO_2 particles are excluded from the current generation process.

In order to establish which is the capacity limiting structural parameter we should consider the changes that take place at the microstructural level of PAM on cycling. These changes were followed by SEM examinations at high magnification of 30,000× and 40,000×.

3.6.3.2. Microstructure. Figs. 13–16 show SEM micrographs of the PAM in the charged state at cycles 35, 100, 180 and 260, respectively. The photographs that present a general view of the aggregate are denoted with (a), those showing the microstructure of the aggregate interior are marked with (b), and those presenting the microstructure of the aggregate surface with (c) and (d). The following conclusions can be drawn from these figures about the evolution of the microstructure of PAM.

1. 35th cycle (Fig. 13): the aggregates are built of numerous agglomerates, which consist of a large number of particles that most often coalesce. Fig. 13b and d show that the aggregates' surface and interior are built from agglomerates. On the aggregate surface the particles are more pronounced, i.e. their boundaries are better defined. PbO_2 needle-like (acicular) particles are formed on the surface of $PbSO_4$ crystals to which H_2SO_4 has a free access. A SEM micrograph of such particles is presented in Fig. 13c.
2. 100th cycle (Fig. 14): a well-pronounced PAM aggregate structure is seen in the figure (Fig. 14a). The particles building up the agglomerates, which form the internal part and the surface of the aggregate, are more

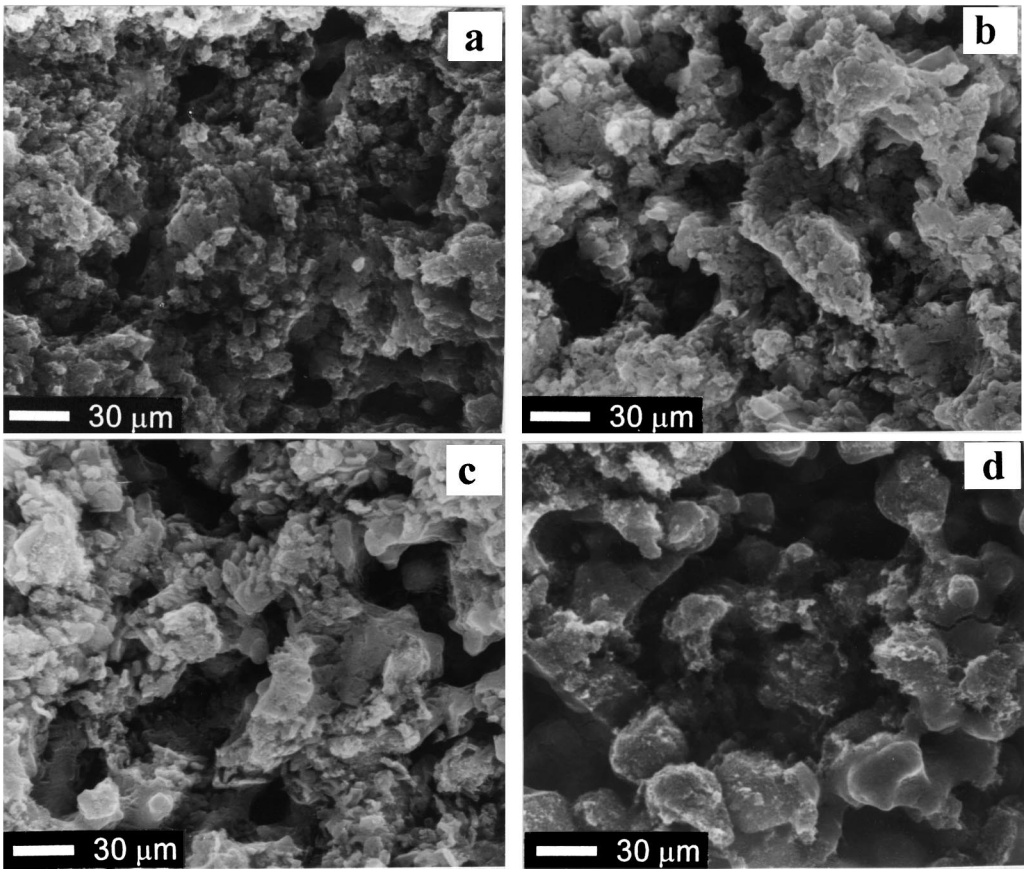

Fig. 12. Macrostructure evolution for charged PAM of plates with Pb–4% Sb grids cycled at high charge rate: (a) 35th cycle; (b) 100th cycle; (c) 180th cycle; (d) 260th cycle.

differentiated from each other (Fig. 14b and d). Some of the needle-like particles are thicker or have coalesced (Fig. 14c). On comparing Figs. 13b and d with 14b and d, it can be seen that the differentiation of the particles building up the agglomerates in the aggregate's interior has increased for 65 cycles.

3. 180th cycle (Fig. 15): the encircled regions in Fig. 15a show that part of the aggregate surface is smooth. A picture of these smooth surface areas at high magnification is presented in Fig. 15d. It shows that they are composed of a large number of PbO_2 particles with crystal forms tightly bound to each other. The agglomerate structural level has vanished. The agglomerates have been transformed into particles of similar sizes. The needle-like crystals also manifest relative individuality (Fig. 15c). The aggregate surface layer of densely packed crystals has micropores of reduced size. It is to be expected that this layer would behave like a membrane layer. Such a membrane layer is expected to highly impede the H_2O, H_2SO_4 and H^+ fluxes moving from a macropore to the aggregate interior and backwards. The participation of PbO_2 from the aggregate's interior in the discharge reaction will be reduced. Hence, the capacity will decline. Fig. 15a shows that such a membrane layer is not formed on the entire surface of all aggregates. At some sites, the agglomerates have not yet fully transformed to particles (Fig. 15b).
4. 260th cycle (end of battery life, Fig. 16): almost all aggregates have acquired a smooth surface (Fig. 16a, encircled regions). The agglomerate structure has disappeared completely. The aggregate surface is covered by a membrane layer (Fig. 16c and d), irrespective of the shape of the constituent particles. This is a serious barrier between the solution in the macropores and the PbO_2 reactant in the interior of the aggregates during discharge. Fig. 16b shows that the agglomerate structure has also disappeared in the interior of the aggregates and has changed into connected individual particles. Large pores are observed in the interior of the aggregate. The membrane is located only on its surface. The agglomerate transformation into particles was observed earlier [22,42]. As a result of disintegration of the agglomerate structure in the particles the contact between the building elements of the structure is impaired. The particles have smaller contact surface and most often it is hydrated, i.e. with high Ohmic resistance. The contact surface between the agglomerates is larger and often the agglomerates

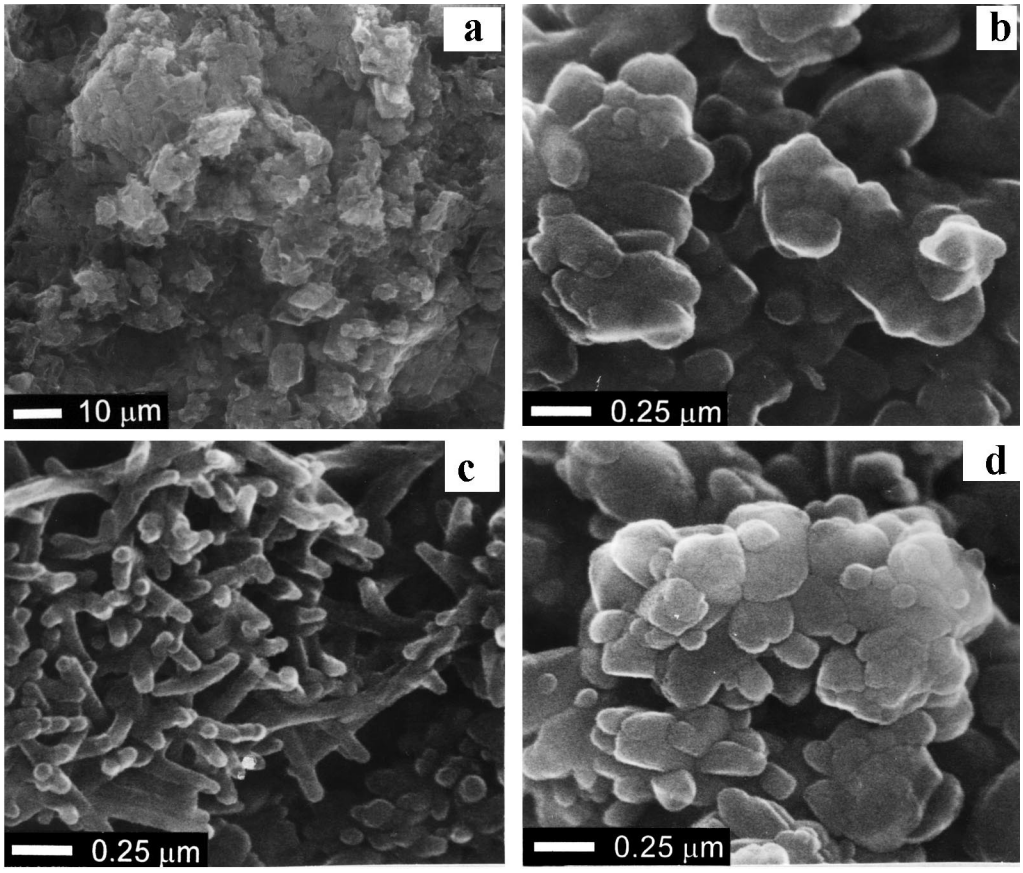

Fig. 13. Microstructure of PAM of plates with Pb–4% Sb grids cycled at high charge rate (cycle 35): (a) general view of the aggregate; (b) microstructure of the aggregate's interior; (c) and (d) microstructure of the aggregate's surface.

coalesce whereby their crystal zones interconnect to form an integral electroconductive network. On disintegration of the agglomerate level this network breaks up and large zones of PAM are excluded from the current generation process, hence the capacity declines.

The formation of aggregates with smooth surface was described earlier by Simon and Caulder [31], Kim et al. [33] and Chang [34]. This structure was named "coralloid". The above authors have established that the coralloid structure has but a limited capacity.

It is interesting to see where are the $PbSO_4$ crystals formed (in the aggregates' interior or on their surface) during the discharge of the above described membrane layer surface. Fig. 17 presents SEM photographs of a discharged PAM after 260 cycles, i.e. at the end of battery life.

- Fig. 17a and b show that the skeleton of PAM aggregates is generally preserved after discharge. However, it has broken at some sites (Fig. 17a, encircled regions). $PbSO_4$ crystals are formed there. Probably, at these sites the surface layer of the aggregate has no membrane structure or the membrane layer has disintegrated and H_2SO_4 has entered the interior of the aggregate and has converted PbO_2 to $PbSO_4$ thus breaking the skeleton.
- $PbSO_4$ crystals are formed in macropores on the surface of the aggregates (Fig. 17b–d).
- Pb^{2+} ions formed as a result of the reduction of PbO_2 at some sites on the aggregates' surface diffuse to $PbSO_4$ crystals and are incorporated into their growth. Consequently, crystals with well defined walls, edges and apexes are formed (Fig. 17c and d).
- However, the reduction process proceeds also in the interior of the aggregates. This may happen if H^+ ions penetrate through the membrane micropores in the aggregates' interior, and H_2O and Pb^{2+} ions pass in the opposite direction, whereas SO_4^{2-} ions cannot penetrate into the interior of the aggregates. These conditions are met only at some sites of the membrane layer. In this case the following reaction of PbO_2 reduction proceeds:

$$PbO_2 + 4H^+ + 2e^- \rightarrow Pb(OH)_2 + H_2O \quad (1)$$

$Pb(OH)_2$ may be dehydrated to PbO. Formation of orthorhom β-PbO on PAM discharge was established through electron micro-diffraction [46]. Part of the Pb^{2+} ions from the interior of the aggregates diffuse through the membrane layer and are deposited onto the $PbSO_4$ crystals. This is a slow process that takes hours to be completed [47]. Fig. 16b

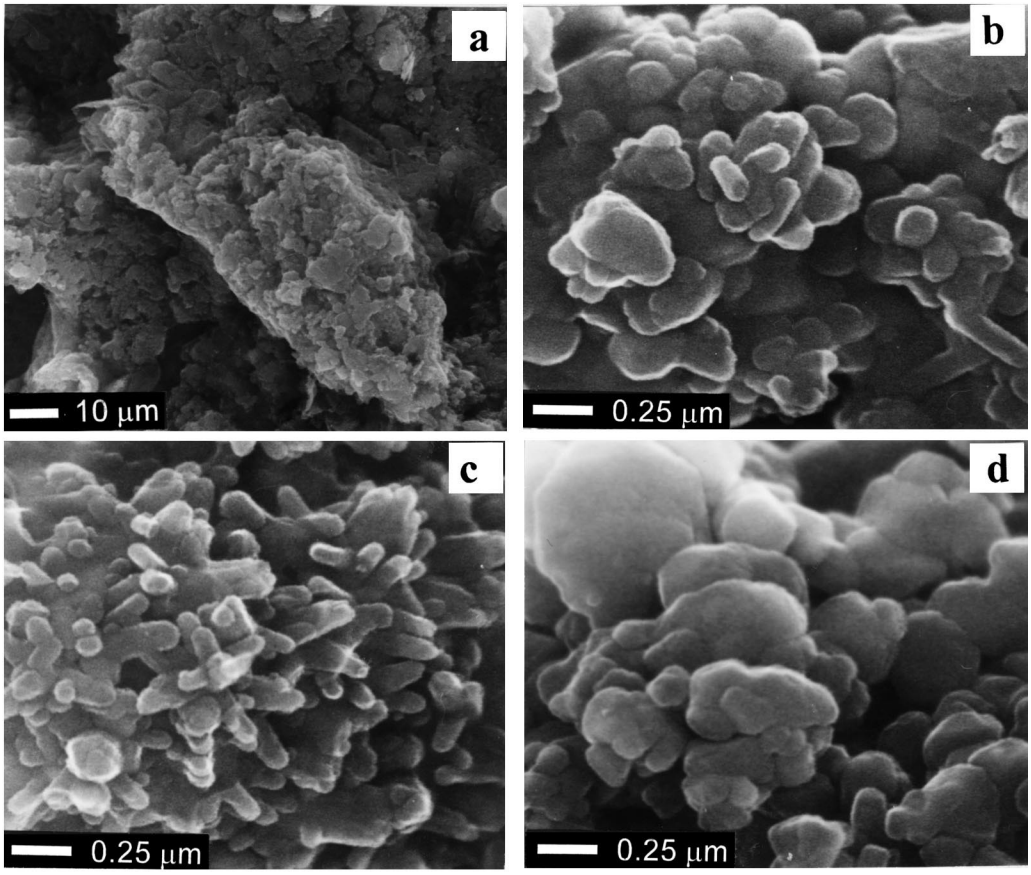

Fig. 14. Microstructure of PAM of plates with Pb–4% Sb grids cycled at high charge rate (cycle 100): (a) general view of the aggregate; (b) microstructure of the aggregate's interior; (c) and (d) microstructure of the aggregate's surface.

shows that large pores are formed in the interior of the PbO_2 aggregates as a result of carrying away of part of the lead material.

At some sites the membrane gradually disintegrates with time under the action of the reduction process. Consequently, H_2SO_4 penetrates into the interior of the aggregates. The reaction of PbO_2 reduction proceeds at an accelerated rate. $PbSO_4$ is formed and the skeleton breaks at these sites. This can be seen in Fig. 17b (the framed region). $PbSO_4$ crystals have been formed on both sides of the broken aggregate.

3.6.4. How far is the formation of aggregate operative structure of PAM a universal phenomenon during cycling?

This could be established through SEM examinations of the microstructure and macrostructure of PAM at the end of battery life. The results of these examinations will be presented below.

3.6.4.1. Battery with Pb grids cycled at slow (20 h) charge. Fig. 18 presents the macro- and microstructures of PAM after 32 cycles (i.e. at the end of battery life). It is evident from the photograph in Fig. 18a that this PAM has well developed both aggregate and macropore systems. The pore volume is 0.17 cm^3/g (Fig. 4). The BET surface area is 2 m^2/g. Fig. 18b shows that the aggregates are rather bushy. The photographs in Fig. 18c and d present the microstructure (40,000×) of the aggregate surface and of its interior, respectively. The agglomerates have transformed into crystallites. Twin crystals are frequently observed. The largest particle size is 500–600 nm. The crystallites have well-shaped faces, apexes and edges. Some of the crystallites have partially built faces of a prismatic form. Several small particles can be distinguished in the interior of these crystals (Fig. 18c). The microstructure is built through contacts between the crystallites' faces. The contact areas are not large. Consequently, a rather delicate electrical and mechanical system is formed in PAM, which could easily be disrupted if the contact areas between the particles are reduced during the discharge. In this case, too, disintegration of the agglomerate structure into particles with crystal shape impairs the electronic contact between the building elements of the structure. Fig. 1a shows that the cycle life of this battery is only 32 cycles. The above crystal type of operative structure is responsible for the short cycle life. The delicate contact between the crystals in PAM, and especially between PAM and the corrosion layer, limits strongly the capacity of the battery.

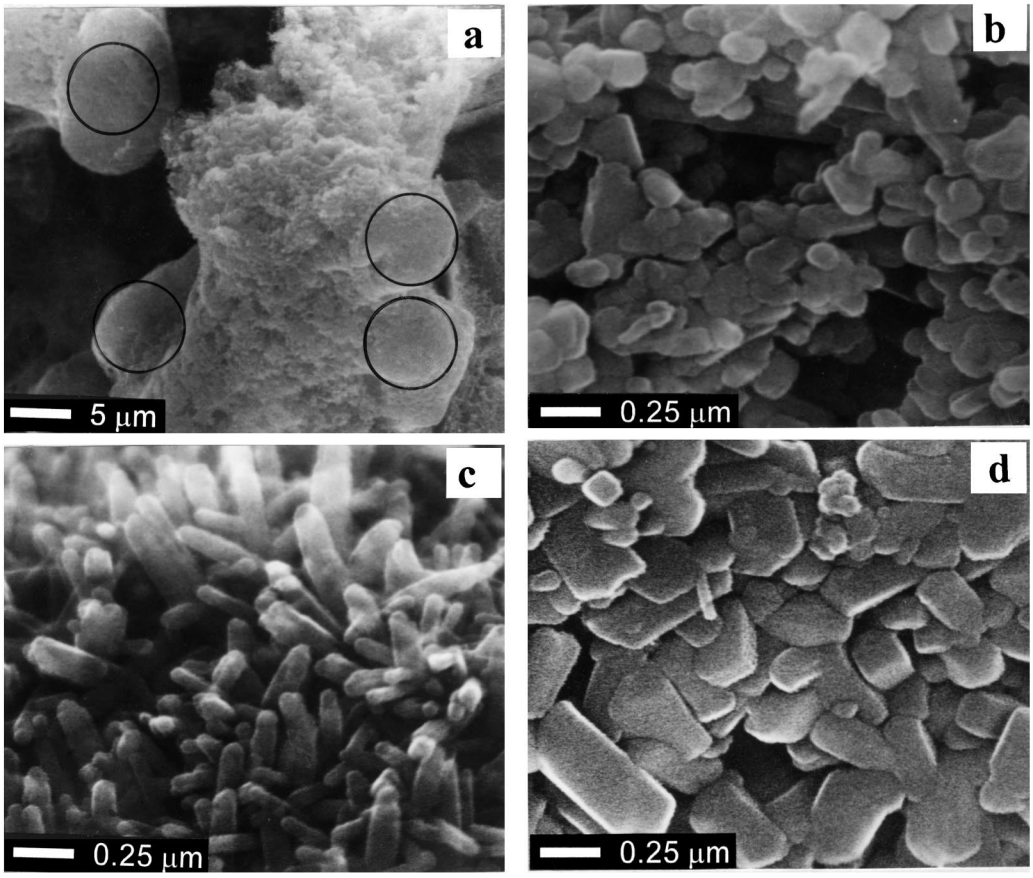

Fig. 15. Microstructure of PAM of plates with Pb–4% Sb grids cycled at high charge rate (cycle 180): (a) general view of the aggregate; (b) microstructure of the aggregate's interior; (c) and (d) microstructure of the aggregate's surface.

3.6.4.2. Batteries with Pb grids cycled at high charge rate. Fig. 19 shows the micro- and macrostructure of PAM at the end of battery life (after 260 cycles). These photographs feature a fairly well developed aggregate structure. According to the porometric data, the pore volume is 0.30 cm^3/g, and the macropores amount to 35% of the total pore volume, the BET surface area is 4.5 m^2/g. Fig. 19 shows quite a large variety of aggregate surface patterns:

1. Aggregates with rough surface (Fig. 19a and b). They are built of individual particles as well as of agglomerates containing several particles. The structure in the aggregates' interior is similar to that on their surface.
2. Aggregates with smooth surface (Fig. 19b). This type of surface is a result of the formation of a crystal membrane (Fig. 19d).
3. In the center of Fig. 19a and c, $PbSO_4$ crystals can be identified on the surface of the aggregates, which are covered with a film from which PbO_2 whiskers grow. This film is probably composed of a four-valent lead compound.

3.6.4.3. Batteries with Pb–4% Sb grids cycled at low charge rate. The micro- and macrostructure of PAM after 460 cycles are presented in Fig. 20. The aggregate structure is dominating (Fig. 20a), part of the aggregates having smooth surface (crystalline membrane layer), while another part has a rough structure. These are the sites of breaking of the PAM pieces to examine the interior of the aggregates. The macroporous system is well developed (Fig. 20a). The pore volume is 0.22–0.23 cm^3/g and remains relatively steady for 200 cycles. The pores with $r > 10$ μm occupy 20% of the pore volume and the micropores ($r < 0.1$ μm) amount to 6%. The BET surface is about 1.5 m^2/g between cycles 50 and 275, and reaches 4 m^2/g thereafter. This increase is due to reduction in crystallite size from 110 to 45 nm (Fig. 7a). Fig. 20 presents two types of particles observed at cycle 460: 70 nm in size (Fig. 20c) and about 225 nm in size (Fig. 20b). The small particles have well pronounced crystalline appearance. This PAM structure could endure a greater number of cycles, but the life of the battery was limited by corrosion of the grids.

3.6.4.4. Battery with PbCaSn grid cycled at high charge rate. Fig. 21 presents SEM micrographs of PAM micro- and macrostructure after the battery reached its end of life (450 cycles). The macrostructure is built of about 10 μm thick

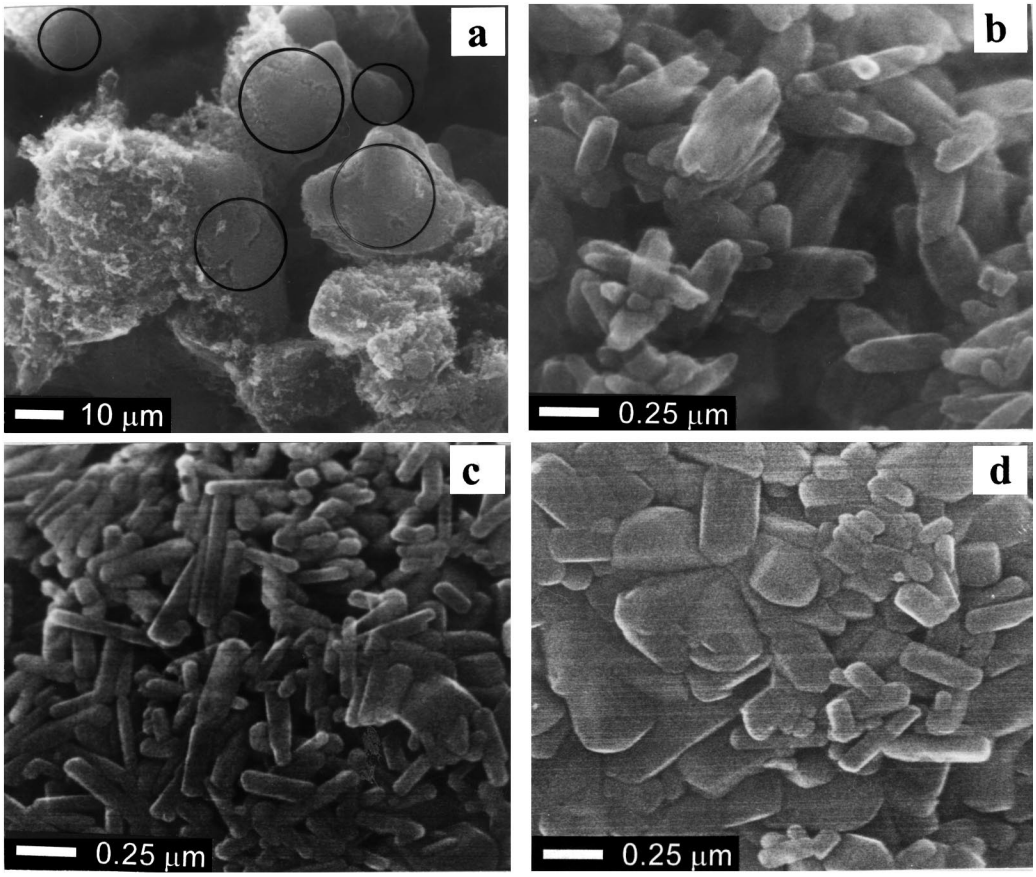

Fig. 16. Microstructure of PAM of plates with Pb–4% Sb grids cycled at high charge rate (cycle 260, end of life): (a) general view of the aggregate; (b) microstructure of the aggregate's interior; (c) and (d) microstructure of the aggregate's surface.

aggregates with rough surface (Fig. 21a). The pore volume is 0.24–0.26 cm^3/g, the volume fractions of pores with $r > 10$ μm being 45%, and of pores with $r < 0.1$ μm, 18%. Fig. 21b shows the microstructure on the aggregate surface.

3.6.4.5. Battery with PbSnCa grids cycled at slow charge regime. The micro- and macrostructure of PAM are presented in Fig. 22a and b, and that of the corrosion layer in Fig. 22c at the end of plate's life (cycle 248). A fairly well organized PAM structure is observed in Fig. 22a. The macrostructure contains aggregates with membrane and rough surfaces. The system of pores is well developed and the pore volume is 0.20–0.23 cm^3/g, the pores with $r > 10$ μm occupying 30% of the pore volume, while those with $r < 0.1$ μm amount to 17%. The microstructure (Fig. 22b) is built of agglomerates comprising coalesced particles. The smallest particles in Fig. 22b have a size of 90 nm. All this indicates that the contact between the agglomerates and the large particles is very good. The BET surface area is 2.2 m^2/g. Fig. 22c shows the structure of the corrosion layer. It features numerous cracks and caves which may impede seriously the passage of the current between PAM and the CL. The interphase layer limits the cycle life to 210 cycles.

3.6.4.6. Battery with PbSnSb grids cycled at high charge rate. Fig. 23 presents SEM photographs of the PAM macro- and microstructure at the end of battery life (440 cycles). The aggregate structure is well developed with membrane and rough appearance of the aggregate surface. The pore volume is 0.22–0.24 cm^3/g of which 45% is occupied by pores with $r > 10$ μm and 20% by pores with $r < 0.1$ μm. Fig. 23b presents the microstructure of the aggregate interior. It is built up of small agglomerates comprising coalesced particles. The size of crystallites is about 60 nm (XRD). The particles contain 0.25 wt.% Sb. It has been established [43,44] that antimony increases the hydrated zones in the particles thus improving the contact between them. Fig. 23b shows that the particles have interconnected to form a continuous microstructure. This structure of PAM is very favorable for long cycle life.

3.6.4.7. Batteries with PbSnSb grids cycled at low charge rate. Fig. 24 presents SEM photographs of PAM at the end of battery life (364 cycles). Channels with cross-section $r > 10$ μm are observed in the macrostructure (Fig. 24a). According to Fig. 5 the pores with radii > 10 μm occupy 65% of the total pore volume. The aggregate structure is quite well developed. The microstructure is formed of

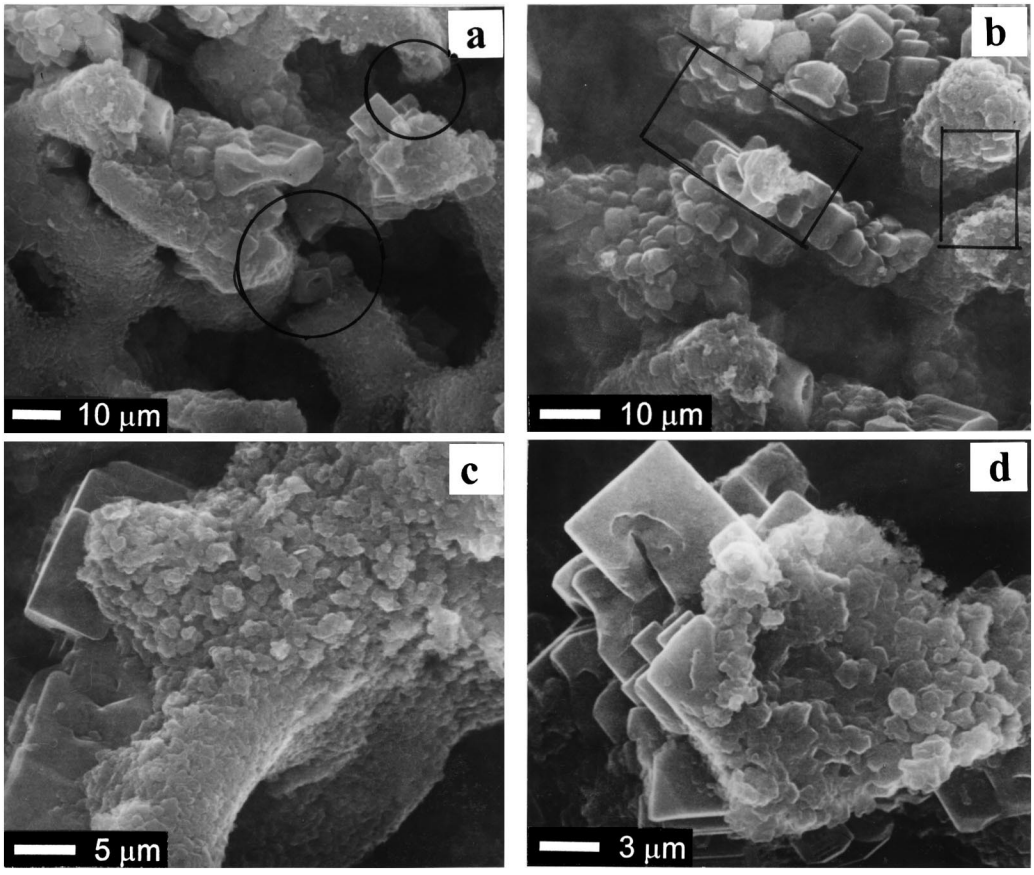

Fig. 17. Macrostructure of PAM of plates with Pb–4% Sb grids cycled at high charge rate (discharged state; cycle 260, end of life).

agglomerates that are built of many coalesced particles (Fig. 24b). This PAM structure has an area of 2 m^2/g, but despite the small surface, the good aggregate skeleton should be capable to ensure a high capacity and long cycle life of the battery. However, it is actually not so long, 360 cycles only. The grid is still ''healthy''. Fig. 24c shows a SEM micrograph of the PAM/CL contact layer. It can be seen that the layer is highly porous and contains large caves and thin aggregates. Probably, part of the material has eroded from the contact layer. If even a small part of PbO_2 in the interphase layer is reduced to $PbSO_4$, this will reduce the cross-section of the aggregates, increase the Ohmic resistance and limit the capacity and cycle life of the battery. Hence, the structure of the interphase layer may limit the capacity during the middle stage of cycling thus setting the beginning of the final period of battery cycle life.

4. Discussion

4.1. General scheme of the operative structure of PAM

Considering the operative macrostructure of PAM presented in Figs. 12–24 we come to the general conclusion that it forms a skeleton built of interconnected aggregates and macropores between them. This skeleton could be determined by the technological structure of PAM. This is the case of the 4BS technology [22]. The transformation of $4PbO{\cdot}PbSO_4$ crystals into PbO_2 aggregates proceeds through metasomatic processes during formation. In this way the aggregate structure is pre-set by the paste precursor. With the 3BS technology the PAM structure looks rather like a porous mass (Fig. 11) and on cycling this structure is converted into aggregates interconnected to build a skeleton. Fig. 25 presents a scheme of the various types of aggregates in the operative structure as deduced from the results obtained in the course of these investigations (Figs. 12–24).

4.2. Influence of PAM microstructure on positive plate cycle life

Table 2 summarizes the mean sizes of the crystallites presented in Fig. 7 as well as the smallest and largest particle sizes measured from the SEM micrographs in Figs. 11–24. The values for the particles bigger than 300 nm are not quite reliable as it is sometimes very difficult to say whether these are single particles or a formation of two coalesced ones. On grounds of the above data we calculated the ratio between

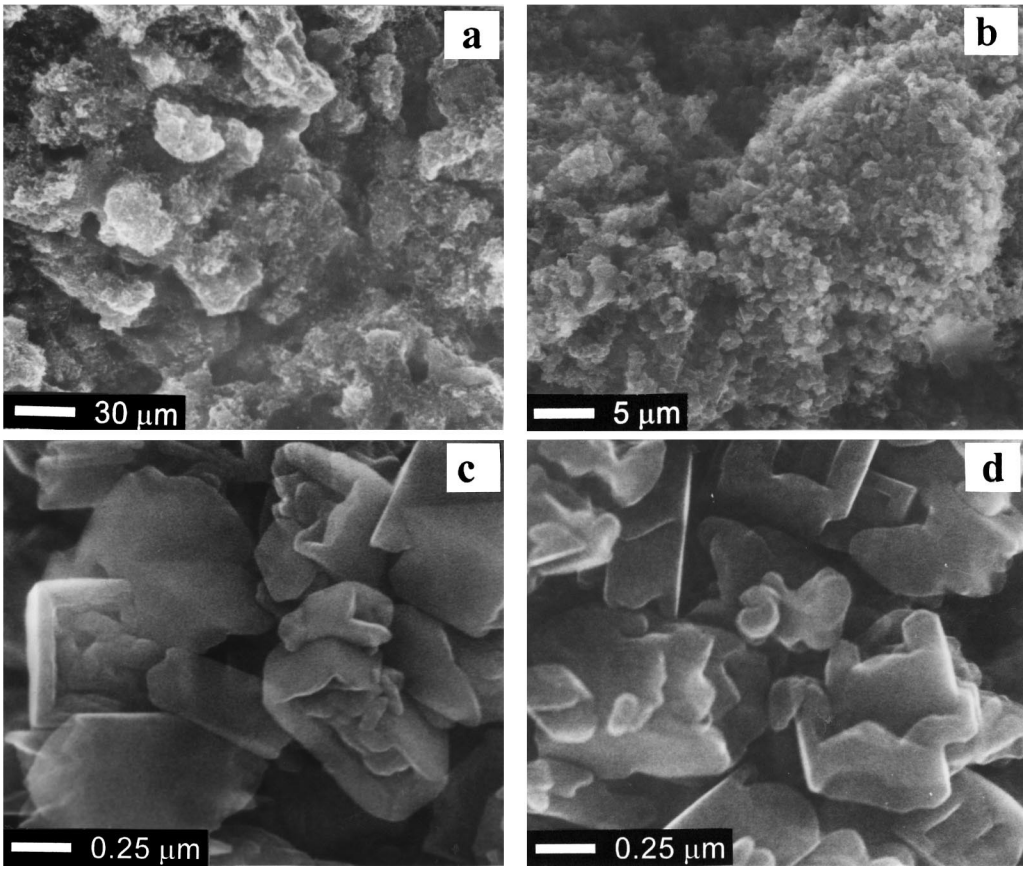

Fig. 18. Structure of PAM of plates with Pb grids cycled at low charge rate (cycle 50, end of life): (a) and (b) macrostructure; (c) and (d) microstructure.

Table 2
Sizes of PbO_2 particles, crystallites, and the ratio between them (PCR)

Plate type	Cycle	Crystallite size (nm)	Sb content (wt.%)	Figure	Small particles		Large particles	
					Particle size (nm)	PCR	Particle size (nm)	PCR
Initial PAM	1	25	–	11	30; 50	1.2; 2.0	150	6.0
Pb (slow)	32	100	–	18c	74; 100	0.75; 1.0	300; 400	3.0; 4.0
				18d	75; 100	0.75; 1.0	450	4.5
PbCaSn (slow)	61–210	95	–	22b	75; 100	0.8; 1.0	250; 230	2.6; 2.4
Pb–4% Sb (slow)	460	45	0.9	20b	75; 100	1.7; 2.2	225; 250	5; 5.5
				20c	75; 100	1.7; 2.2	150–400 needles	
PbSbSn (slow)	360	75	0.1	24b	100	1.3	175; 225	2.3; 3.0
Pb (fast)	260	45	–	19d	100	2.2	200; 250	4.4; 5.5
PbCaSn (fast)	450	60	–	21b	75; 125	1.25; 2.0	225; 275	3.75; 4.6
Pb–4% Sb (fast)	35	38	0.08	13b	120	3.15	250	6.5
				13c	75	2.0	300	7.9
	100	44	0.1	14b	75; 100	1.7; 2.3	250	5.7
				14d	100	2.3	225; 300	5.1; 6.8
	180	60	0.18	15b	75; 100	1.25; 1.7	225; 250	3.75; 4.20
				15d	100; 125	1.7; 2.1	200; 325	3.3; 5.4
	260	50	0.24	16b	75; 50	1.5; 1.0	175; 200	3.5; 4.0
				16c	50/300		50/500	4.5; 5.0
				16d	50; 75 needles	1.0; 1.5	225; 225 needles	3.2; 3.6
PbSbSn (fast)	440	62	0.2	23d	75; 85	1.2; 1.37	200; 225	3.2; 3.6

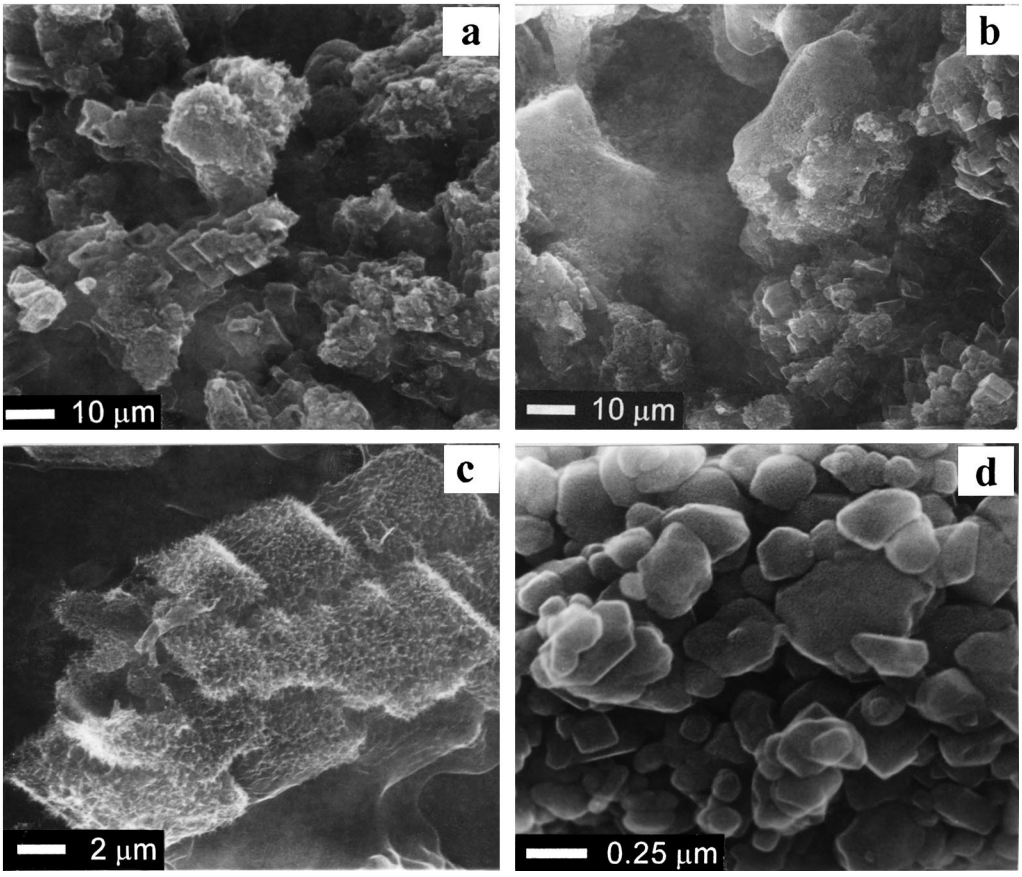

Fig. 19. Structure of PAM of plates with Pb grids cycled at high charge rate (cycle 260, end of life).

the size of the particles and the size of their crystallites. Let us denote this ratio as PCR (particle/crystal ratio). The obtained PCR values are also given in Table 2.

The particles in the PAM obtained on Pb and PbSnCa grids at low charge rate have PCR < 1.0. This has no physical meaning. Probably, these are amorphous (hydrated) particles, i.e. there are no crystallites in them. Many of the particles with PCR $= 1$ are spherical or close to spherical in shape. We have not examined their structure, but their outer shape (similar to a water drop) implies that these are gel-like particles. It can be assumed that the crystallization processes have not yet started in these particles.

The influence of PAM microstructure (size of crystallites and of large and small particles) on battery cycle life is illustrated in Fig. 26. The batteries with Pb grids cycled at low charge rate have PAM composed of large crystallites ($\sim$100 nm) and large particles sized between 300 and 400 nm. The SEM micrographs presented in Fig. 18c and d show that the particles have well pronounced crystal shapes. The life of these batteries is only 32 cycles.

The battery with PbSnCa grids cycled at low charge rate has a cycle life of 62 cycles and its PAM comprises 92 nm crystallites and large particles sized between 225 and 250 nm. Tin (and maybe Ca as well) have reduced the size of the β-PbO_2/$PbO(OH)_2$ particles.

When Ca in the PbSnCa grid alloy is substituted with Sb and the battery is cycled at low charge rate the size of the crystallites decreases to 75 nm (Fig. 26) and that of the large particles is between 175 and 225 nm. This battery has a cycle life of 360 cycles.

Fig. 26 shows also that the PAM of the battery with Pb–4% Sb grids when cycled at low charge rate comprises crystallites 45 nm in size and large particles sized between 175 and 250 nm. The cycle life of this battery is 475 cycles. Antimony has reduced substantially the size of the crystallites.

When the above four types of batteries are cycles at high charge rate, their positive active masses are composed of crystallites sized between 45 and 60 nm and large particles with sizes within the range 175–275 nm. The cycle life of these batteries is between 250 and 450 cycles.

The above results indicate that there is no direct linear dependence between the size of crystallites and particles in PAM and the battery cycle life.

Table 3 summarizes the PCR values obtained for the batteries under test. When the batteries with Pb, PbSnCa and PbSnSb grids are cycled at high charge rate their PAM particles contain a greater amount of crystallites than the PAM particles of the same batteries but cycled at low charge rate. The cycle life of the batteries is longer when the fast charge mode is employed. The reverse situation is observed

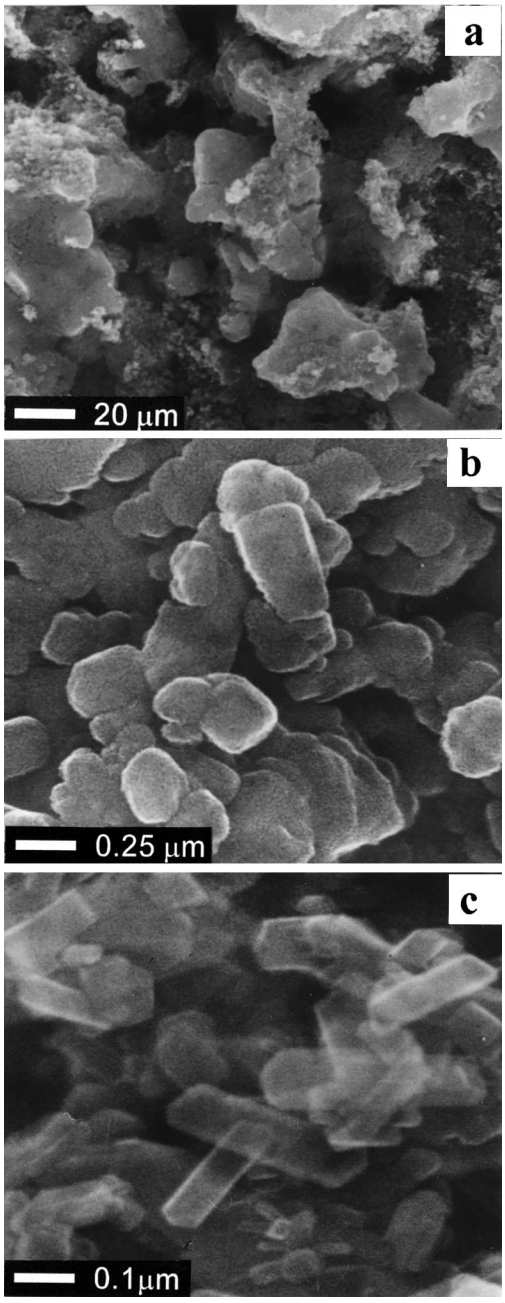

Fig. 20. Structure of PAM of plates with Pb–4% Sb grids cycled at low charge rate (cycle 460, end of life).

with the PbSb battery, however. In this case, the PCR value is higher for the PAM obtained on slow charge cycling. The cycle life of this battery is longer when cycled at low charge rate. The exception confirms the rule. This is due to the high content of Sb (0.9%) incorporated into the PAM particles. This effect of increased number of crystallites in the particles may be associated with the electrical properties of PbO_2/$PbO(OH)_2$ particles. The crystal zones (these contain the crystallites) are degenerated semi-conductors with high electron conductivity. When the crystal zones in the particles, agglomerates and aggregates are interconnected into a network, the electron transfer between the interphase layer

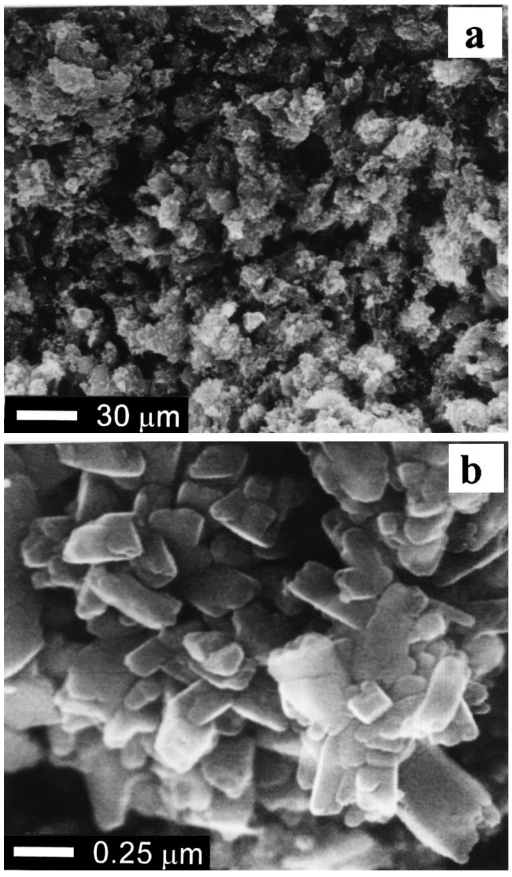

Fig. 21. Structure of PAM of plates with PbCaSn grids cycled at high charge rate (cycle 450, end of life): (a) macrostructure; (b) microstructure.

and each spot in PAM is facilitated. The greater number of crystallites in the particles (both large and small) facilitates the interconnection between the crystal zones of the individual particles, i.e. the formation of an integral network of crystal zones in PAM and thus improves its electron conductivity.

Hence, the crystal zones in the PAM particles and their interconnections will influence the capacity and cycle life of the positive plates. However, it should be emphasized that

Table 3

Battery type	Slow charge		Fast charge	
	Cycle life	PCR	Cycle life	PCR
Large particles				
Pb	32	3.0–4.5	260	4.4–5.5
PbSnCa	61	2.6–2.4	450	3.75–4.60
PbSb	460	5.0–5.5	260	3.50–5.0
PbSnSb	360	2.3–3.0	440	3.20–3.6
Small particles				
Pb	32	0.75–1.0	260	2.2
PbSnCa	61	0.8–1.0	450	1.25–2.0
PbSb	460	1.7–2.2	260	1.0–1.5
PbSnSb	360	1.3	440	1.20–1.37

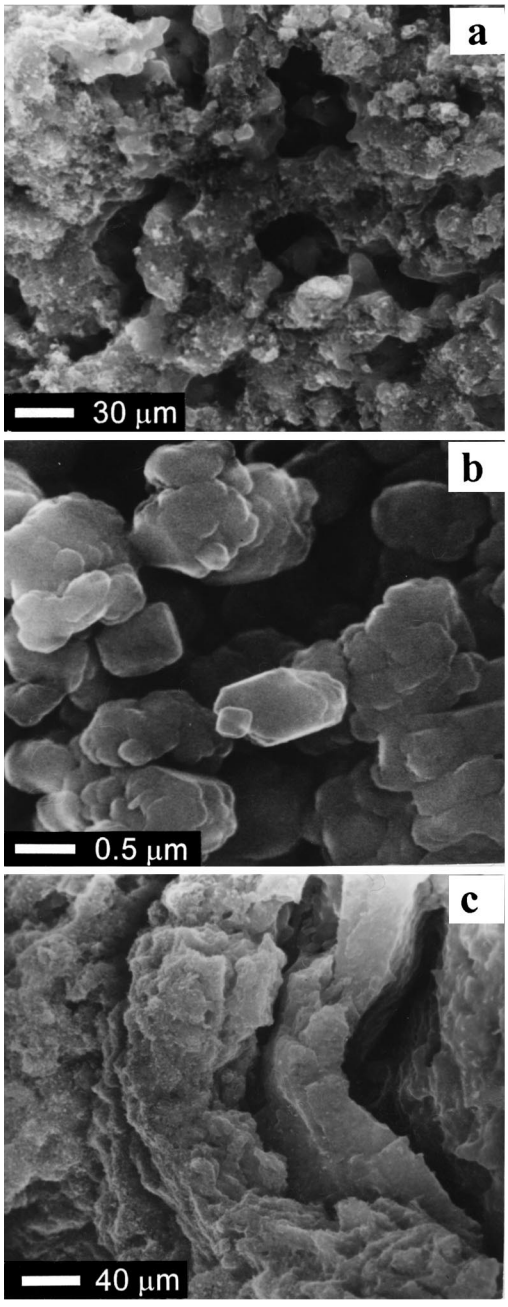

Fig. 22. PAM samples from the plate with PbCaSn grid cycled at low charge rate (cycle 248, end of life): (a) PAM macrostructure; (b) PAM microstructure; (c) corrosion layer.

the above parameter (PCR) is not the only one determining the capacity and cycle life performance of the positive plates. This is the parameter through which the microstructure of PAM affects the capacity and cycle of the battery.

4.3. Mechanism of the chemical and electrochemical processes during charge

As evidenced by the above discussed experimental results, the charging current, i.e. the rate of the electrochemical reaction(s), is of utmost importance for the capacity and cycle life performance of positive plates with Sb-free grids. Why does the kinetics of the charge process affect the life of the plates? This effect is realized through the type of PAM structure that is formed on charge as a result of the kinetics of the charge processes, i.e. the electrochemical reactions as well as the physico-chemical and crystallization processes.

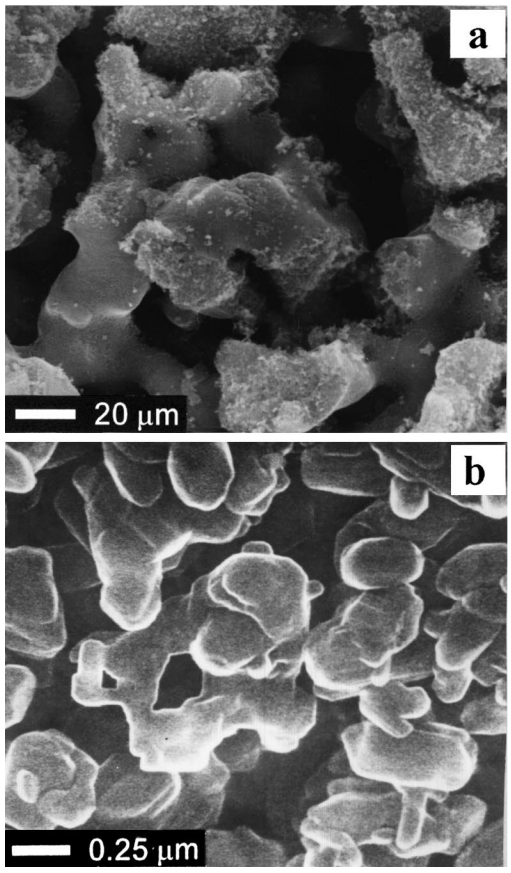

Fig. 23. Structure of PAM of plates with PbSbSn grids cycled at high charge rate (cycle 440, end of life): (a) macrostructure; (b) microstructure.

Recently, we proposed the following sol–gel–crystalline mechanism of the charge processes [45,46]. It involves chemical and electrochemical reactions:

$$PbSO_4 \Leftrightarrow Pb^{2+} + SO_4{}^{2-} \quad (2)$$

$$Pb^{2+} \rightarrow Pb^{4+} + 2e^- \quad (3)$$

$$Pb^{4+} + 4H_2O \rightarrow Pb(OH)_4 + 4H^+ \quad (4)$$

$Pb(OH)_4$ has a sol character. It dehydrates partially, as a result of which gel particles are formed:

$$n[Pb(OH)_4] \Leftrightarrow [PbO(OH)_2]_n + nH_2O \quad (5)$$

$[PbO(OH)_2]_n$ stands for a gel particle. A further dehydration process takes place and crystallites and crystal zones of PbO_2 are formed in single particles or particles coalesced into agglomerates.

$$[PbO(OH)_2]_n \Leftrightarrow \underset{\text{crystal zones}}{[k(PbO_2)} + \underset{\text{gel zones}}{(n-k)PbO(OH)_2]_n} + kH_2O \quad (6)$$

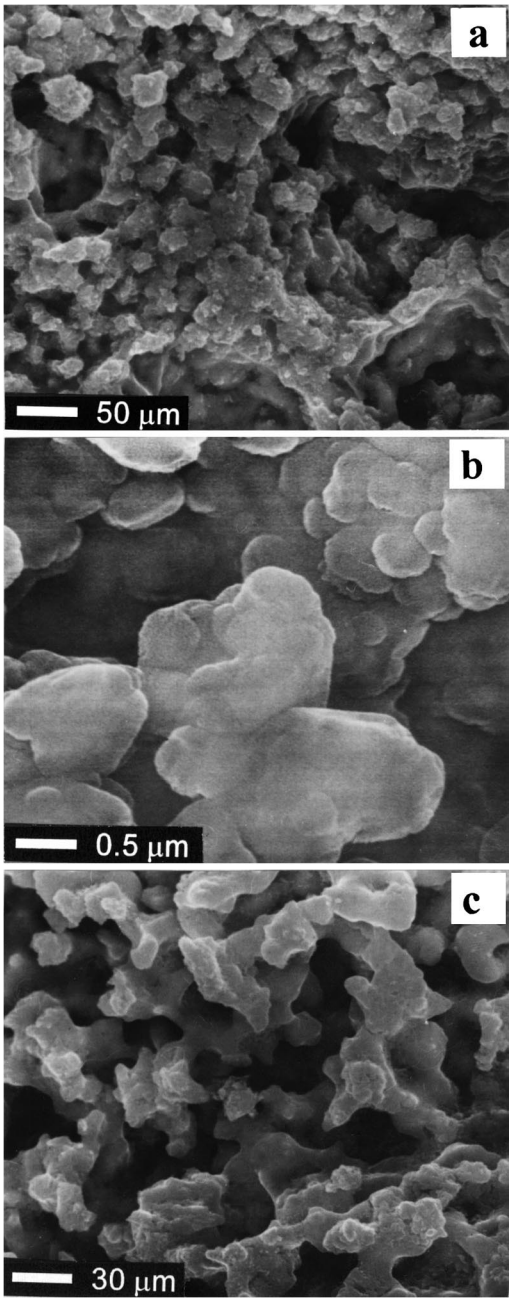

Fig. 24. Structure of PAM of plates with PbSbSn cycled at low charge rate (cycle 364, end of life): (a) bulk PAM macrostructure; (b) bulk PAM microstructure; (c) contact PAM/CL interface.

When the $PbSO_4$ crystal is not passivated, reaction (2) proceeds rapidly and a high concentration gradient is created in the pores. The electrochemical reaction (3) is generally a fast reaction. The rate of reaction (4) depends on the concentration of Pb^{4+} ions and H_2O molecules. At high current densities, the concentration of Pb^{4+} ions is high and reaction (4) proceeds at a high rate. The rate of reaction (5) is determined by the concentration of $Pb(OH)_4$ molecules in the pores. They will determine the number and size of the gel particles, which will be formed. At high rate of reaction (3), i.e. at high current densities, a great number of gel particles are formed. The dehydration reactions (5) and (6) release water, whether reaction (4) consumes water. The pores have a relatively small volume and reaction (4) will use up the water released by reactions (5) and (6), thus shifting the equilibrium reactions (5) and (6) to the right, i.e. the processes of dehydration will be accelerated. These processes will also depend on the flow of H_2O coming from the bulk of the electrolyte. If this flow is small and the current density is high, the dehydration processes will proceed at a high rate. Consequently, a great number of crystallites and crystal zones will be formed.

Fig. 26 shows that fast charge cycling yields smaller particles than those formed on slow charge, and the data in Table 3 indicate that the number of crystallites in the particles is greater in the PAM obtained on fast charge cycling as compared to that formed on slow charge.

At low charge rate, the supersaturation of the $Pb(OH)_4$ sol in the pores is small and there is sufficient time for growth of large particles with crystalline forms. The crystallization processes that take place in the particles and agglomerates result in the formation of well-pronounced crystalline forms. These processes are clearly manifested in pure Pb plates (see Fig. 18).

Reactions (4)–(6) are also affected by the temperature and the foreign ions (dopants). The latter are incorporated into the gel particles and may influence both the rates of reactions (4)–(6), and the ratio between gel and crystal zones in the particles. Sb and Sn are such dopants. They increase the amount of hydrated zones in the particles [48,49] and reduce the size of the crystallites in them (Fig. 7). On fast charge and in the presence of 0.2% Sb in PAM, the PbO_2 crystallites are sized about 60 nm (Fig. 9). On slow charge and at the same Sb content (0.2%) in PAM, the crystallites have a size of 100 nm (Fig. 9). Crystallites of the same size (105 nm) are observed in the PAM of Pb batteries obtained on slow charge (Fig. 7). Hence, 0.2% Sb content in PAM has almost no influence on the size of the crystallites formed on slow charge cycling. Fig. 7 shows that on increase of the Sb content in PAM above 0.2% the size of the crystallites formed on slow charge decreases and at 0.9% Sb content, crystallites sized about 45 nm are formed. Hence, the influence of Sb on the size of PbO_2 crystallites depends not only on its concentration, but also on the rates of reactions (4)–(6), i.e. on the conditions of charge.

For reaction (3) to proceed at a given site in the volume of PAM an electronic contact between this site in PAM and the current collector should be ensured. Let us cal these sites in PAM ''active centers''. The crystal zones of PbO_2 have high electronic conductivity, whereas $PbO(OH)_2$ gel zones are electron and proton conductors with a resistance much higher than that of the PbO_2 crystal zones. Consequently, the active centers will be formed at those sites that have the least electronic resistance. During the initial period of cycling, the active centers will be distributed through the technological structure. Depending on the type, location and number of active centers a conversion of the technological

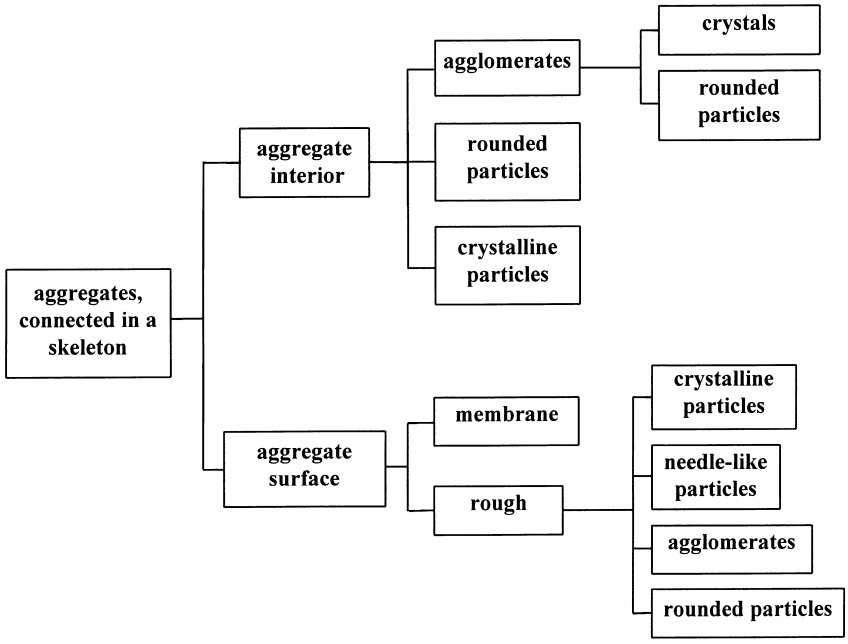

Fig. 25. Scheme of PAM structure.

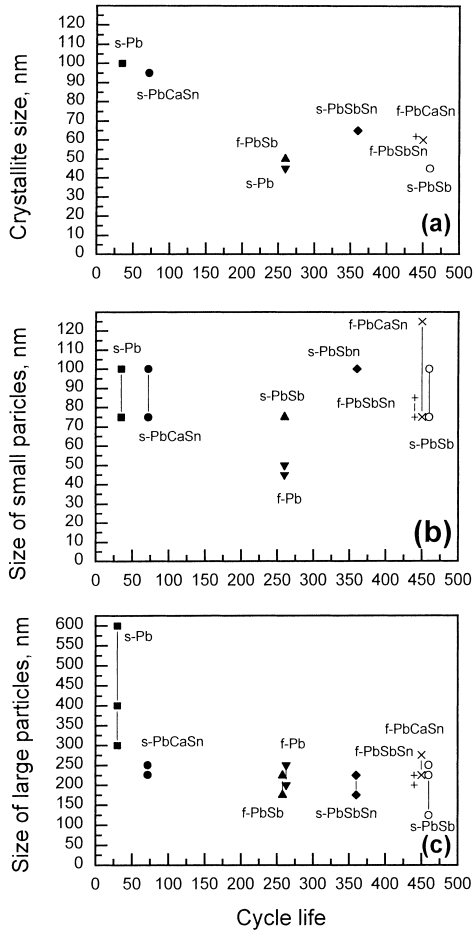

Fig. 26. Crystallite and particle size vs. battery cycle life.

structure into operative one will occur and the latter will develop further on cycling.

4.4. Phenomena that limit the cycle life of the positive plates

The cycle life of the positive lead acid battery plates is determined by a number of phenomena that occur in the three structural elements of the plate: grid, interphase layer and PAM. The phenomena that limit the life of the plates are schematically presented in Fig. 27. Depending on the possibilities of every structural element to participate in the charge/discharge processes, it could become a capacity or life limiting parameter.

1. *Grid*: it becomes a capacity limiting parameter when it breaks or when the cross-section of the grid bars decreases by more than 30%. On battery cycling, the grid takes over the pulsations of PAM and if it is not mechanically strong, it creeps. When its expansion exceeds 5%, the contact between the grid and PAM is interrupted and the battery loses capacity [50].
2. *Interphase layer*: this layer connects the grid with PAM and it consists of a corrosion layer formed as a results of oxidation of the grid metal and contact layer of the active mass [41]. The interphase layer may limit the life of the positive plate when the technological structure of the interphase layer is converted into an inefficient operative structure. This leads to PCL effect. However, the interphase layer may also cause failure of the battery during the middle period of its life. For example, in the

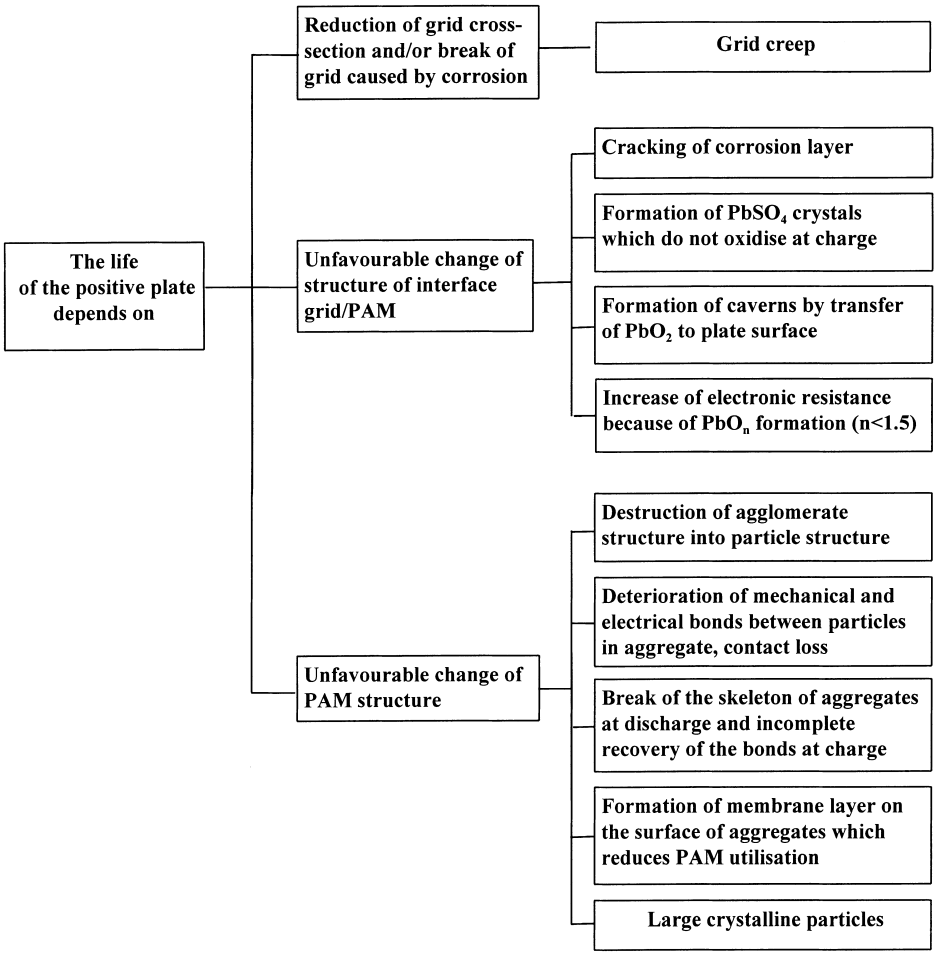

Fig. 27. Failure modes of positive plates related to their different structural components.

following cases:

- when a corrosion layer with a strongly cracked layered structure is formed (Fig. 22c);
- when the aggregates which connect the PAM with the corrosion layer become very thin (Fig. 24c);
- when caverns are formed in the interphase layer;
- when, during discharge, the aggregates that connect PAM with the corrosion layer are reduced faster than the PAM to PbO_n ($n < 1.5$); PbO_n has high resistance and hence the polarization of the plate will increase rapidly.

The influence of the structure of the interphase layer on the capacity was considered earlier [38].

3. *PAM*: the processes of charge and discharge do not proceed at equal rate throughout the volume of PAM [38]. During discharge, certain zones in PAM are excluded, for one reason or another, from the current generation process. The reasons for exclusion of these PAM zones may be:
   - when the agglomerates building up the aggregates disintegrate into separate particles with weaker contact between them, which have high resistance and/or can easily break;
   - when the structure of PAM comprises predominantly large PbO_2 crystals with not very good contact between them (Fig. 18);
   - when the skeleton of PAM is broken at some sites or there are cracks in it where $PbSO_4$ crystals are formed (Fig. 17a);
   - when the surface of some of the aggregates is covered with a membrane layer with very small pores thus practically excluding considerable amounts of PbO_2 crystals building these aggregates from the current generation process;when $PbSO_4$ crystals oxidize only on their surface during charge forming a thin PbO_2 layer, which can be easily reduced thus breaking the current circuit.

Part of the above outlined phenomena lead to irreversible capacity loss (e.g. disintegration of the grid structure, formation of large caverns in the interphase layer, cracking or breaking of the PAM skeleton, etc.) and hence short cycle life. Another part of the above phenomena are reversible and the battery may restore its capacity. This can be achieved through the use of high charge current (RIMU) [23] or through the introduction of appropriate additives.

In Section 4.2, we discussed the influence of high charge current on the microstructure of PAM. However, the capacity is often limited by phenomena that proceed in the macrostructure of PAM and in the interphase layer.

At high charge currents, a sufficient number of agglomerates and particles are formed, which integrate into the skeleton and can connect the broken branches electrically and mechanically recovering the skeleton's integrity. In this way the cracked and broken branches of the skeleton are ''welded''. Thus, the skeleton structure is re-built, which ensures long middle period of battery life.

At low charge currents, the reactions proceed at preferred sites (active centers) only. At these sites the conditions for reactions (2)–(6) are the most favorable. These reactions proceed at a low rate and do not always lead to the formation of aggregates that can be integrated into the skeleton or ''weld'' its broken branches. Hence, the recovery of the skeleton of PAM and of the interphase layer is not always guaranteed. Some zones of PAM may lose their electronic contact with the interphase layer. This leads to a gradual loss of capacity on cycling (Fig. 2a).

It follows that the life of the positive plates depends on the stability and quality of the mechanical and electrical connections between the aggregates as well as on the integrity of the skeleton of PAM and of the interphase layer.

On charge and discharge, a competition between the processes in the bulk of PAM and in the interphase layer takes place. The role of the interphase layer in determining battery life increases with decrease in cross-section and number of aggregates in the layer that connect the PAM with the interphase layer. This can be seen in Fig. 24c. Besides, the formation of groups of $PbSO_4$ crystals in the interphase layer which are not oxidized to PbO_2 also increase the role of this layer in determining battery life. The beneficial effect of high charge current on the process of restoration of the PAM structure is also valid for the structure of the interphase layer. As discussed above, Sb and Sn have a similar effect on the integrity of the crystal zones at the microstructural level of PAM. Moreover, these dopants improve the electroconductivity of the branches in the interphase layer.

5. Conclusions

Through experimental investigations of the changes in structural parameters of the positive plates with Pb, Pb–4% Sb, PbCaSn and PbSbSn grids, cycled with high and low charging currents, the following were established:

- The porosity of PAM increases gradually to a maximum of 0.28 cm^3/g. The volume of micropores decreases whilst that of macropores increases. This allows better access of the H_2SO_4, H_2O and H^+ fluxes to the interior of the plate and to the interphase layer. The role of the interphase layer as a capacity limiting element increases.
- The size of crystallites in the particles and agglomerates increases to such a level that particles with crystalline forms begin to grow. This phenomenon is most pronounced in the batteries with Pb grids when cycled at low charge rate.
- When the grid alloy contains Sb the latter is gradually accumulated in PAM. On slow battery charge, when the Sb content in PAM exceeds 0.2 wt.%, the size of crystallites and particles decreases and at 0.9% Sb content in PAM the crystallites have a size of 45 nm.
- The operative structure of PAM consists of aggregates (branches) built of agglomerates and/or individual particles. On cycling, the agglomerates disintegrate into particles. These particles can form a membrane layer on the surface of the aggregates, which impedes the access of H^+, SO_4^{2-} ions and H_2O fluxes to the aggregates interior and may limit plate life.

When the crystallization processes in PAM particles and agglomerates become dominant (mainly at slow charge), large particles are formed with crystalline forms, which have delicate contact between them and may reduce the capacity of PAM and limit the life of the battery. By keeping the crystallite size smaller than 60 nm, the interparticle contact is preserved intact. This could be achieved either by applying high charging currents $I > 1$ C or by using crystal growth rate modifiers such as Sb and Sn in appropriate concentrations.

On discharge, some processes occur that cause the branches (aggregates) of the skeleton to break and so large zones of PAM may be excluded from the current generation processes. On charge, the skeleton is re-built, partially or entirely, thus making it one of the structural elements influencing the life of the battery.

The influence of charging current on the structure of PAM, and hence on plate life, is interpreted on grounds of the sol–gel–crystal mechanism of the processes that proceed on charge.

The above-described phenomena taking place on cycling provide a sound background for making some conclusions of practical significance.

If the battery is prepared with pure Pb or Sb-free alloy grids, it should be charged with an initial charging current higher than 1.5 C to enable the formation of such a PAM structure that would ensure long cycle life.

If the battery is charged with a low initial current, then the PAM or the grid alloy must contain Sb or SnSb. Probably, some other metals may have analogous influence on the PAM structure. If the above requirement is met, the life of the positive plates may be prolonged and it will be limited by corrosion of the grid.

The combination of charge regime and dopants in PAM could improve significantly the cycle life performance of the battery.

Acknowledgements

The authors acknowledge with thanks the financial support provided by Japan Storage Batteries Ltd. for implementation of part of the research included in this work. We are also thankful to our colleague L. Bogdanova for the technical assistance and to Dr. K. Micka for the useful discussion.

References

[1] U. Hullmeine, A. Winsel, E. Voss, J. Power Sources 25 (1989) 27.
[2] A. Winsel, E. Voss, U. Hullmeine, J. Power Sources 30 (1990) 209.
[3] E. Meissner, E. Voss, J. Power Sources 33 (1991) 231.
[4] E.M. Valeriote, D.M. Jochim, J. Power Sources 40 (1992) 93.
[5] E. Meissner, H. Rabenstein, J. Power Sources 40 (1992) 157.
[6] T.G. Chang, E.M. Valeriote, D.M. Jochim, J. Power Sources 48 (1994) 163.
[7] L.T. Lam, H. Ozgun, O.V. Lim, J.M. Hamilton, L.H. Vu, D.G. Vella, D.A.J. Rand, J. Power Sources 52 (1995) 215.
[8] M. Calabek, K. Micka, P. Baca, P. Krivak, V. Smarda, J. Power Sources 62 (1996) 161.
[9] M. Calabek, K. Micka, D. Baca, P. Krivak, V. Smarda, J. Power Sources 64 (1997) 123.
[10] K. Takahashi, M. Tsubota, K. Yonezu, K. Ando, J. Electrochem. Soc. 130 (1983) 2144.
[11] A.F. Hollenkamp, J. Power Sources 59 (1996) 87.
[12] K. Fuchida, K. Okada, S. Hattory, M. Kono, M. Yamane, T. Takayama, J. Yamashita, J. Nakayama, ILZRO, Project LE-276, Report nos. 7 and 8, Research Triangle Park, NC, USA, 1982.
[13] J. Burbank, J. Electrochem. Soc. 111 (1964) 1112.
[14] H.K. Giess, in: K.R. Bullock, D. Pavlov (Eds.), Proceedings of the Symposium on Advances in Lead Acid Batteries, Vol. 84-14, Electrochemical Society, Pennington, NJ, USA, 1984, p. 241.
[15] D. Pavlov, B. Monachov, M. Maja, N. Penazzi, J. Electrochem. Soc. 136 (1989) 27.
[16] D. Pavlov, A. Dakhouche, T. Rogatchev, J. Power Sources 30 (1990) 117.
[17] E. Voss, J. Power Sources 24 (1988) 172.
[18] U. Hullmeine, E. Voss, A. Winsel, J. Power Sources 30 (1990) 99.
[19] E. Ritchie, J.J. Burbank, J. Electrochem. Soc. 117 (1970) 299.
[20] E. Meissner, J. Power Sources 67 (1997) 135.
[21] P. Lailler, F. Zaninotto, S. Nivet, L. Torcheux, J.-F. Sarrau, J.P. Vaurijoux, D. Devillier, J. Power Sources 78 (1998) 204.
[22] D. Pavlov, E. Bashtavelova, J. Electrochem. Soc. 131 (1984) 1468.
[23] J. Yamashita, Y. Matsumaru, J. Appl. Electrochem. 18 (1988) 595.
[24] J. Yamashita, H. Yufu, Y. Matsumaru, J. Power Sources 30 (1990) 13.
[25] R.J. Hill, I.C. Madsen, J. Electrochem. Soc. 131 (1984) 1487.
[26] S.M. Caulder, J.S. Murday, A.C. Simon, J. Electrochem. Soc. 120 (1973) 1515.
[27] J.D. Jorgensen, R. Varma, F.J. Rotella, G. Cook, N.P. Yao, J. Electrochem. Soc. 129 (1982) 1687.
[28] R.J. Hill, A.M. Jessel, I.C. Madsen, in: K.R. Bullock, D. Pavlov (Eds.), Proceedings of the Symposium on Advances in Lead Acid Batteries, Vol. 84-14, Electrochemical Society, Pennington, NJ, USA, 1984, p. 59.
[29] R.J. Hill, J. Power Sources 22 (1988) 175.
[30] R.J. Hill, J. Power Sources 25 (1989) 313.
[31] A.C. Simon, S.M. Caulder, J. Electrochem. Soc. 118 (1971) 659.
[32] J. Perkins, M.T. Coyle, J. Electrochem. Soc. 124 (1977) 524.
[33] I. Kim, S.H. Oh, H.Y. Kang, J. Power Sources 13 (1984) 99.
[34] T.G. Chang, J. Electrochem. Soc. 131 (1984) 1755.
[35] J. Bouet, J.P. Pompon, Electrochim. Acta 26 (1981) 1477.
[36] E. Bashtavelova, A. Winsel, J. Power Sources 46 (1993) 219.
[37] A. Winsel, E. Bashtavelova, J. Power Sources 73 (1998) 242.
[38] D. Pavlov, G. Petkova, M. Dimitrov, M. Shiomi, M. Tsubota, J. Power Sources 87 (2000) 39 .
[39] D. Pavlov, J. Power Sources 48 (1994) 179.
[40] M. Dimitrov, D. Pavlov, J. Power Sources 48 (1994) 179.
[41] D. Pavlov, J. Power Sources 53 (1995) 9.
[42] D. Pavlov, E. Bashtavelova, J. Electrochem. Soc. 133 (1986) 241.
[43] D. Pavlov, I. Balkanov, T. Halachev, P. Rachev, J. Electrochem. Soc. 136 (1989) 3189.
[44] D. Pavlov, J. Electrochem. Soc. 139 (1992) 3075.
[45] D. Pavlov, I. Balkanov, P. Rachev, J. Electrochem. Soc. 134 (1987) 2390.
[46] D. Pavlov, E. Bashtavelova, D. Simonsson, P. Ekdunge, J. Power Sources 30 (1990) 77.
[47] D. Pavlov, E. Bashtavelova, V. Iliev, Proceedings of the 32nd Meeting of ISE, Part I, Dubrovnik, Yugoslavia, 1981, p. 146.
[48] B. Monahov, D. Pavlov, J. Electrochem. Soc. 141 (1994) 2316.
[49] D. Pavlov, I. Balkanov, J. Electrochem. Soc. 139 (1992) 3075.
[50] H. Giess, J. Power Sources 53 (1995) 31.